# Physicochemical characterization of free troposphere and marine boundary layer ice-nucleating particles collected by aircraft in the eastern North Atlantic

Daniel A. Knopf[1,2], Peiwen Wang[1], Benny Wong[1,2], Jay M. Tomlin[3], Daniel P. Veghte[4†], Nurun N. Lata[4], Swarup China[4], Alexander Laskin[3], Ryan C. Moffet[5], Josephine Y. Aller[1], Matthew A. Marcus[6], Jian Wang[7]

[1]School of Marine and Atmospheric Sciences, Stony Brook University, Stony Brook, NY 11794, USA
[2]Department of Chemistry, Stony Brook University, Stony Brook, NY 11794, USA
[3]Department of Chemistry, Purdue University, West Lafayette, IN 47907, USA
[4]Environmental Molecular Sciences Laboratory/Pacific Northwest National Laboratory, Richland, WA 99354, USA
[5]Sonoma Technology, Inc., Petaluma, CA 94954, USA
[6]Advanced Light Source, Lawrence Berkeley National Laboratory, Berkeley, CA 94720, USA
[7]Center for Aerosol Science and Engineering, Department of Energy, Environmental and Chemical Engineering, Washington University in St. Louis, St. Louis, MO 63130, USA

†Current address: Center for Electron Microscopy and Analysis, The Ohio State University, Columbus, OH 43212, USA

*Correspondence to*: Daniel A. Knopf (daniel.knopf@stonybrook.edu)

**Abstract**

Atmospheric ice nucleation impacts the hydrological cycle and climate by modifying the radiative properties of clouds. To improve our predictive understanding of ice formation, ambient ice-nucleating particles (INPs) need to be collected and characterized. Measurements of INPs at lower latitudes in a remote marine region are scarce. The Aerosol and Cloud Experiments in the Eastern North Atlantic (ACE-ENA) campaign, in the region of the Azores Islands, provided the opportunity to collect particles in the marine boundary layer (MBL) and free troposphere (FT) by aircraft during the campaign's summer and winter intensive operation period. The particle population in samples collected was examined by scanning transmission X-ray microscopy with near-edge X-ray absorption fine structure spectroscopy. The identified INPs were analyzed by scanning electron microscopy with energy-dispersive X-ray analysis. We observed differences in the particle population characteristics in terms of particle diversity, mixing state, and organic volume fraction between seasons, mostly due to dry intrusion events during winter, and between the sampling locations of the MBL and FT. These differences are also reflected in the temperature and humidity conditions under which water uptake, immersion freezing (IMF), and deposition ice nucleation (DIN) proceed. Identified INPs reflect typical particle types within the particle population on the samples and include sea salt, sea salt with sulfates, and mineral dust, all associated with organic matter, and carbonaceous particles. IMF and DIN kinetics are analyzed with respect to heterogeneous ice nucleation rate coefficients, $J_{het}$, and ice nucleation active site density, $n_s$, as a function of the water criterion $\Delta a_w$. DIN is also analyzed in terms of contact angles following classical nucleation theory. Derived MBL IMF kinetics agree with previous ACE-ENA ground site INP measurements. FT particle samples show greater ice nucleation

propensity compared to MBL particle samples. This study emphasizes that the types of INPs can vary seasonally and with altitude depending on sampling location, thereby showing different ice nucleation propensities, crucial information when representing mixed-phase cloud and cirrus cloud microphysics in models.

**Short Summary (500 character in total)**

Ambient particle populations and associated ice-nucleating particles (INPs) were examined from particle samples collected onboard aircraft in the marine boundary layer and free troposphere in the Eastern North Atlantic during summer- and wintertime. Chemical imaging shows distinct differences in the particle populations seasonally and with sampling altitudes which are reflected in the INP types. Freezing parameterizations are derived for implementation in cloud-resolving and climate models.

## Introduction

Ice formation by atmospheric particles affects cloud formation, cloud albedo, and precipitation and, thus, the global radiative budget and the hydrological cycle (Boucher et al., 2013; Storelvmo, 2017; Mülmenstädt et al., 2015; McCoy et al., 2022; Mülmenstädt et al., 2021; McCoy et al., 2020; Murray and Liu, 2022). Supercooled droplets can freeze spontaneously via homogeneous nucleation when temperatures are below ~−38 °C while ice-nucleating particles (INPs) can initiate heterogeneous ice nucleation at higher temperatures and under saturated and subsaturated conditions (Pruppacher and Klett, 1997; Cantrell and Heymsfield, 2005; Knopf et al., 2018; Vali et al., 2015; Kanji et al., 2017; Knopf and Alpert, 2023). Although atmospheric INPs are scarce, typically on the order of 1 in ~$10^5$ ambient particles in a liter of air in the troposphere (DeMott et al., 2010), INPs play an central role in cloud microphysical processes (Peter et al., 2006; Baker, 1997; Storelvmo, 2017; Murray and Liu, 2022). Nevertheless, our predictive understanding of which atmospheric particles act as INPs under conditions typical of mixed-phase clouds in which ice crystals and supercooled liquid droplets coexist and cirrus clouds where only ice crystals exist, is still insufficient. Therefore, the implementation of parameterizations for INP number concentration predictions in cloud and climate models remains challenging (Boucher et al., 2013; Storelvmo, 2017; Cesana and Del Genio, 2021; McCoy et al., 2016; Murray and Liu, 2022). One possible explanation for this is the insufficient characterization of the ambient particles' ice nucleating properties and knowledge of dominant types of INPs in various atmospheric environments (Kanji et al., 2017; Knopf et al., 2018; Cziczo et al., 2017b; Knopf and Alpert, 2023).

The Eastern North Atlantic (ENA) is a region of complex aerosol sources and diverse aerosol composition (Wood et al., 2015; Zheng et al., 2018). Aerosol sources which contribute to the ENA aerosol include natural emissions from the ocean, anthropogenic emissions and biomass burning from North America, and high mineral dust-laden air masses from the Sahara (Wood et al., 2015; Zheng et al., 2020; Alonso-Perez et al., 2012; Zheng et al., 2018; China et al., 2017; Lata et al., 2021).

From June 2017 to February 2018, the Aerosol and Cloud Experiments in the Eastern North Atlantic (ACE-ENA) campaign consisting of airborne deployments and a stationary Atmospheric Radiation Measurement Climate Research Facility

was conducted on Graciosa Island in the Azores (Knopf et al., 2022; Wang et al., 2022; Zawadowicz et al., 2021; Tomlin et al., 2021; Wang et al., 2021). The overarching goals of the ACE-ENA campaign were to advance our understanding of MBL clouds through field measurements of cloud condensation nuclei (CCN), drizzle, and cloud microphysics, to close knowledge gaps in aerosol and cloud processes, and to validate and improve retrieval algorithms of surface-based remote sensing (Wang et al., 2022). Although the focus of this campaign was on liquid cloud processes, it provided a unique opportunity to examine airborne-collected particles in the marine boundary layer (MBL) and free troposphere (FT) as potential sources of INPs in a remote region that is also impacted by aerosol sources far away. During the wintertime, this region also experiences dry intrusion events (DI) from the FT into the MBL (Ilotoviz et al., 2021; Raveh-Rubin, 2017). Since DIS originate from the lower stratosphere or upper troposphere and adiabatically descend, they are associated with dry airmasses that will mix with the MBL moist air (Ilotoviz et al., 2021; Raveh-Rubin, 2017). DIs, in turn, will also transport particles into the MBL thereby impacting the composition of the MBL particle population (Tomlin et al., 2021). The acquired airborne measurements also allowed comparison to previously conducted ground-site INP measurements in this region (Knopf et al., 2022; China et al., 2017; Lata et al., 2021).

In the MBL of ENA, sea spray aerosol (SSA) dominates in the large mode particles, while entrained FT particles from anthropogenic sources contribute to most of the Aitken and accumulation mode particles (Zheng et al., 2018), the latter impacting cloud microphysical properties (Wang et al., 2020). It has been observed that long-range transported and aged wildfire aerosol in the ENA MBL can serve as CCN and, thus, impact local cloud formation (Zheng et al., 2020). During the ACE-ENA campaign elevated CCN number concentrations in the FT were observed that did not impact the MBL CCN pool significantly (Wang et al., 2021). However, entrainment of particles too small to act as CCN from the FT into the MBL can act as CCN after condensational growth. Wang and colleagues further concluded that surface measurements overestimate the number of CCN relevant to the formation of MBL clouds under decoupled conditions (Wang et al., 2021). *Tomlin et al.* (2021) employed single-particle micro-spectroscopic techniques to examine the external and internal mixing state for airborne-collected particle populations sampled during the ACE-ENA campaign. They found that carbonaceous particles were the dominant type in this region, while DI events significantly impacted the particle population by changing the carbonaceous and inorganic contributions. DI events resulted in a decreased contribution of organic compounds to the population in the MMBL and FT while increasing the contribution of inorganic species. This in turn has a direct effect on the particles' hygroscopicity and thus CCN properties. *Tomlin et al.* (2021) concluded that entrainment of particles from long-range continental sources alters the mixing state of the particle population and the CCN properties of aerosol particles in this region.

Less information about INPs in the ENA region is available (Welti et al., 2023). However, since ACE-ENA was conducted in a remote marine region, nascent or aged SSA is well known to have associated organic matter (OM) (Pham et al., 2017; Aller et al., 2017; Facchini and O'Dowd, 2009; O'Dowd et al., 2004; Cochran et al., 2017; Lee et al., 2020; Ault et al., 2013a; Alpert et al., 2015) which can serve as INPs (Cornwell et al., 2021; McCluskey et al., 2018; McCluskey et al., 2017; DeMott et al., 2016; Alpert et al., 2022; Ladino et al., 2016; Wilson et al., 2015; Knopf et al., 2011; Alpert et al., 2011a; Alpert et al., 2011b; Schnell and Vali, 1976; Schnell, 1975; Wilbourn et al., 2020; Irish et al., 2019; Creamean et al., 2019; Cornwell

et al., 2019) and thus would be expected to contribute to the regional INP pool (Lata et al., 2021; Knopf et al., 2022; China et al., 2017). Other sources of particles which might contribute to the INP population include long-range transported carbonaceous particles and dust particles originating from the north African deserts as well as primary organic aerosol particles from, e.g., fossil fuel combustion and biomass burning (Knopf et al., 2018; Kanji et al., 2017). Secondary organic aerosol (SOA) originating from anthropogenic and biogenic precursor gases have been shown to initiate ice formation (Kanji et al., 2017; Wang et al., 2012a; Wolf et al., 2020; Knopf et al., 2018). Finally, while mineral dust particles are well known to be some of the most efficient inorganic INPs for temperatures lower than -20 °C (e.g., Murray et al., 2012; Kanji et al., 2017; Cziczo et al., 2017a), OM or biological material associated with soil dust particles can also serve as potent INPs active above -10 °C (Kanji et al., 2017; Knopf et al., 2021; Hill et al., 2016; Creamean et al., 2020; Tobo et al., 2014).

*China et al.*, (2017) report on the examination of particles collected at the Observatory of Mountain Pico 2225 m above sea level located on a neighboring Azores Island, which were studied for their propensity to initiate immersion freezing (IMF) and deposition ice nucleation (DIN). IMF describes the process of ice nucleation from an INP immersed in a supercooled liquid droplet while DIN represents the ice formation pathway where ice forms from the supersaturated vapor phase directly on the INP (Knopf et al., 2018; Vali et al., 2015). Though recent studies show that DIN could be the result of pore condensation freezing, where homogeneous freezing in nanometer-sized pores is facilitated at lower relative humidity with respect to ice ($RH_{ice}$) than needed for homogeneous ice nucleation (David et al., 2019; Marcolli, 2014, 2020). *China et al.* (2017) demonstrated that most particles were coated by OM and that the identified INPs were mixtures of dust, aged sea salt and soot, and that the OM was acquired either at the source or during transport. Furthermore, they showed that ice formation was promoted by both IMF and DIN pathways. These findings have been corroborated in a recent study that also examined particle samples collected at the Observatory of Mountain Pico using micro-spectroscopic analyses of the ambient particle population and INPs (Lata et al., 2021). In this study, IMF and DIN measurements were related to the size-resolved chemical composition, mixing state (MS), distribution of OM, functional groups, and phase state of the ambient particle population. In the case of identified and characterized INPs, particulate OM, sulfate content, and phase state were found to influence the properties of INPs (Lata et al., 2021). Specifically, highly viscous particles showed a greater propensity to initiate DIN at temperatures below 220 K compared to less viscous (liquid-like) particles. To relate the physicochemical properties of the particle population to the identified INPs, *Knopf et al.* (2022) analyzed particle samples collected at the ACE-ENA ground site during summer 2017 ~~to relate the physicochemical properties of the particle population with the identified INPs~~. The identified INP types were found to consist of fresh sea salt with organic compounds or processed sea salt containing dust and sulfur with organic compounds and showed the same organic spectral features as SSA INPs (Alpert et al., 2022; Knopf et al., 2022). That recent study supports the contention put forth by *Knopf et al.*(2022), that the MBL can serve as a source of IMF and DIN INPs.

Results reported in this study extend previous INP measurements of ambient particles collected during ACE-ENA (Knopf et al., 2022) examining particle samples collected in the MBL and FT regions by aircraft during summer and winter and in the presence and absence of DI events. We analyzed 7 particle samples collected during 6 different flights including 3 samples from the MBL and 4 from the FT which allows for examination of the role of dynamics (transport and 4 DI events),

sampling location, and season in determining the physicochemical properties of the aerosol population and INPs. Additionally, analysis of these aircraft collected samples will be compared to ground site aerosol and INP measurements conducted during the same field campaign (Knopf et al., 2022). Scanning transmission X-ray microscopy with near-edge X-ray absorption fine structure spectroscopy (STXM/NEXAFS) is used to determine the organic speciation, MS, and organic volume fraction (OVF) of the individual particles thereby characterizing the particle population in each sample. Scanning electron microscopy with energy dispersive X-ray analysis (SEM/EDX) is used to examine the morphology and elemental composition of the identified INPs which are then placed in context with the investigated particle population. The thermodynamic conditions, i.e., temperature (T) and $RH_{ice}$, at which collected particles induce IMF and DIN are assessed. The ice nucleation kinetics of IMF and DIN kinetics will be assessed using the classical nucleation theory (CNT) rooted water-activity based immersion freezing model (ABIFM) (Knopf and Alpert, 2013) and the ice nucleation active sites (INAS) approach (Vali, 1971; Connolly et al., 2009). The acquired ice nucleation kinetics will be compared to IMF and DIN kinetics descriptions made on particle samples collected at the ACE-ENA ground site during summer 2017 (Knopf et al., 2022). These are applied to derive formulations of corresponding IMF and DIN parameterizations applicable to MBL and FT aerosol of the ENA region. Since particle sampling onto substrates for different analyses proceeded in series, not exactly the same air masses and particles could be sampled on the different substrates. Additionally, only a limited number of samples could be examined in detail. For these reasons, the results of this study may not bey valid for all instances of MBL and FT and for entire seasons. However, as demonstrated, the results indicate that there are significant differences in the makeup and ice nucleation propensity among samples collected in the MBL and FT and for different seasons. These new data further motivate the need of long-term studies of INP sources in remote regions such as the Azores.

## 2. Experimental methods

### 2.1 Particle collection

Particle sampling for the ACE-ENA campaign has been described in detail in *Tomlin et al.* (2021) and, thus, is only briefly summarized here. Particles were collected aboard the U.S. Department of Energy Gulfstream aircraft (G-1) by impaction onto ~~various~~ substrates. Typical flight patterns were flown between Terceira Island and Graciosa Island, Portugal, and within 20–30 km of Graciosa Island (Tomlin et al., 2021; Wang et al., 2022). The aerosol was provided at 1 SLPM (standard liter per minute) by an isokinetic inlet installed on the G-1 aircraft to a time-resolved aerosol collector (TRAC) a single-stage impactor sealed against ambient conditions with an aerodynamic cut-off diameter, $D_{50\%}$ = 0.36 µm. The TRAC houses a substrate disc that holds up to 160 substrates for collection of particles via impaction at preset time intervals (Tomlin et al., 2021; Laskin et al., 2006; Laskin et al., 2003). The collected particle sizes typically varied between 0.1 and 5 µm. After all substrates are used, the particle samples were removed under particle-free conditions in the laboratory and stored in transmission electron microscopy (TEM) grid boxes in a low humidity storage cabinet (Knopf et al., 2022; Knopf et al., 2021; Tomlin et al., 2021; Knopf et al., 2014).

In this study, we employed $Si_3N_4$-coated silicon wafer chips (Silson Ltd.) for ice nucleation experiments and TEM grids (copper 400 mesh grids, carbon type-B film, Ted Pella, Inc.) for SEM/EDX and STXM/NEXAFS analyses (Knopf et al., 2022; Knopf et al., 2021; Charnawskas et al., 2017).

Table 1 provides sampling date, time, and altitude of the particle samples discussed in this study. S and W indicate the intensive operation periods during the summer and winter, respectively. TRAC impacts particles onto only one substrate for each collection time interval. Hence, collection of particles onto different substrates for examination using different analytical techniques at the same time is not possible. Therefore, substrates for INP measurements and for particle composition do not exactly reflect the same air mass. The difference in sampling heights and collection times are given in Table 1. Table 1 also provides estimated MBL heights derived from flight altitude versus potential temperature plots given in Fig. S1. Regions in which the potential temperature remains nearly constant are indicative of the convective mixed planetary boundary layer (Stull, 1988). For W-FT3-DI the MBL seems to have been mostly decoupled with varying heights throughout the day. We assigned samples originating from the MBL and FT if sampling of the substrates occurred mostly below and above the estimated MBL height, respectively. In some instances, STXM/NEXAFS measurements performed on two TEM grids were combined. Collection periods that were impacted by DI events are indicated in Table 1. DI events are defined by air masses that experience a pressure increase of 400 hPa within a 24 h window within 3° radius around Graciosa Island (Tomlin et al., 2021; Ilotoviz et al., 2021; Raveh-Rubin, 2017). DI events in the ENA region are most common during the winter times. The examined summertime collected (IOP1) samples were not affected by DI events. Figures S2 and S3 present ensemble 10-days HYSPLIT backward trajectory calculations at the sample location during flight (Stein et al., 2015). During summer MBL measurements (S-MBL1), the air masses resided in the MBL for most of the backward trajectory analysis. However, during wintertime MBL sampling flights (W-MBL1-DI and W-MBL2), the trajectories indicate that air masses also originated from the FT. These trends coincide with the identified DI events. For summer FT sampling (S-FT1), the trajectories indicate that the air masses resided for a couple of days at similar altitudes and may have been influenced by MBL air masses after longer times. For wintertime FT sampling (W-FT1-DI, W-FT2, W-FT3-DI), air masses resided for a few days at similar altitudes but at later times originated from higher altitudes. For wintertime FT sampling W-FT1-DI and W-FT3-DI, the air masses originated from higher altitudes coinciding with identified DIs. For the case of W-FT2, however, backward trajectories indicate that air masses resided for longer time at similar altitudes. Qualitatively, there seems to be different trends in the air mass trajectories for sampling times during summer and winter. This is mostly due to the presence of midlatitude DIs (Ilotoviz et al., 2021; Raveh-Rubin, 2017). Four out of the 5 winter sampling periods were impacted by DIs where air descended from the upper troposphere towards the sample location.

**2.2 Single-particle analysis by X-ray and electron microscopy**

STXM/NEXAFS (Kilcoyne et al., 2003) which allows speciation of the particulate organic carbon (OC), and assessment of the particulate OVF was employed to examine the MS of the collected particle population. This microscope was operated at the carbon K-edge (278–320 eV) to enable physicochemical characterization of the particle composition at a spatial resolution of ~35 nm following our previous studies (Knopf et al., 2022; Knopf, 2023; Knopf et al., 2021; Tomlin et al., 2021;

Knopf et al., 2014; Laskin et al., 2019; Laskin et al., 2016; Moffet et al., 2013; Wang et al., 2012b; Moffet et al., 2010; Knopf et al., 2010; Fraund et al., 2020). Since we compare ACE-ENA airborne particle samples with ground site samples published recently (Knopf et al., 2022), STXM/NEXAFS measurements and analysis follow the procedures outlined in this previous study (Knopf et al., 2022). We performed two types of analyses to either examine a larger number of particles or acquire a more detailed analysis of fewer particles. STXM images were recorded at four selected X-ray energies at 35 nm resolution and 1 ms dwell time including 278 eV (pre-edge, inorganic: IN), 285.4 eV (C=C, elemental carbon: EC), 288.5 eV (COOH: OC), and 320 eV (post-edge). This analytical procedure allows imaging of the chemical composition and determination of the MS and OVF of the individual particles (Knopf et al., 2022; Moffet et al., 2010; Hopkins et al., 2007; Fraund et al., 2020). We used NaCl and adipic acid species as representative mass absorption coefficients for the IN and OC particle fractions, respectively (see also discussion in *Fraund et al.*, 2019). The accuracy of the representation of the particle population depends on the number of particles analyzed. For example, if the aim is to describe the probability of different particle-type classes to be at least 0.95 (or at a significance level of 5%) that all particle-type-class estimates are within 0.05 (or 5 %) of the actual population proportions (i.e., the different particle-type classes on the sample), then a sufficient sample size of randomly chosen particles is 510 particles (Thompson, 1987). This statistical analysis allows us to estimate the uncertainty of the particle population's proportions for any given significance level (here, 5 %) and examined particle number. In this study, sample sizes for STXM analysis varied between 71 to 352 particles, resulting in uncertainties of the particle population proportion (i.e., a particle-type class) of about 13 % and 6 %, respectively. Choosing a lower significance level or having a greater sample size will increase or decrease those uncertainties, respectively. In our case, if, e.g., 30 % of the particles are identified as being organic carbon-inorganic mixtures (OCIN), the uncertainty in how representative that particle-type class is, will be ±6.5 % and ±3 % in examination of 71 and 352 particles, respectively. In addition, for selected particles high-resolution energy absorption (NEXAFS) spectra examining 96 energies at 35 nm pixel resolution and 1 ms dwell time were recorded allowing for a detailed interpretation of the particulate OC including organic functionalities.

Particles that were identified as INPs in our ice nucleation experiments by optical microscopy, were individually examined by SEM/EDX for morphological features and elemental composition in a similar fashion as in our previous studies (Knopf et al., 2022; China et al., 2017; Knopf et al., 2014). The SEM/EDX was operated at 20 kV (FEI Quanta 3D, EDAX Genesis). Besides recording electron micrographs for imaging purposes, analysis of the EDX spectra allows quantification of the relative atomic fractions of the following elements: C, N, O, Na, Mg, Al, Si, P, S, Cl, K, Ca, Mn, and Fe.

For analysis of the ice nucleation kinetics, accurate particle surface area is needed. In addition to particle surface area estimates based on optical microscopy, we used particle surface area estimates obtained by computer-controlled SEM/EDX (CCSEM/EDX) (Tomlin et al., 2021) due to its superior resolution compared to optical microscopy (Table 2). When available, these data were acquired from samples collected during the same flights at similar altitudes as the particle samples investigated for this study (Table 1). For each individually analyzed particle, CCSEM/EDX provides an area equivalent diameter (AED) which represents a circle with a diameter that has the same surface area as the imaged particle. The AED is used to estimate the total particle surface area present in the ice nucleation experiments by assuming the particles to be half spheres. As

discussed in *Knopf et al.* (2022), underestimation of the actual particle surface area due the presence of nanoscale surface features would imply that derived ice nucleation kinetics represent upper limits.

### 2.3 Optical microscopy-based ice nucleation experiment

Particles collected on the $Si_3N_4$ coated Si wafer chip substrates were investigated for their ability to serve as INPs at given T and $RH_{ice}$. A custom-built ice nucleation cell which includes a cryo-cooling stage coupled to an optical microscope was used to examine IMF and DIN for temperatures as low as 200 K and up to water saturation (Alpert et al., 2022; China et al., 2017; Charnawskas et al., 2017; Wang et al., 2012b; Knopf et al., 2011). This setup allows one to set the temperature of the substrate, thereby controlling the particle temperature. Inside the cell a humidified flow of ultra-high purity dry nitrogen at 1 standard liter per minute supplies the desired water partial pressure. As the gas passes through and exits the nucleation cell, its dew point is determined using a chilled mirror hygrometer. Substrate temperature and dew point yield $RH_{ice}$. Water uptake and ice formation can be identified by changes in particle size and morphology when the changes are greater than 1 and 0.2 µm in size at magnifications of 230× and 1130×, respectively (Wang and Knopf, 2011). The dew point temperature uncertainty is ± 0.15 K. The uncertainties for $RH_{ice}$ depend on the probed temperature region and range from about ± 4.0 to ± 5.7 % where the uncertainty increases for lower substrate temperatures. The substrate temperature is calibrated by measuring the melting points of different organic species and ice (Rigg et al., 2013). In addition, controlled ice crystal growth and sublimation experiments are conducted to verify the substrate temperature uncertainty (Wang and Knopf, 2011).

A typical experiment starts at subsaturated conditions, i.e., $RH_{ice} < 100\%$. Then $RH_{ice}$ is increased by ~ 2 % $min^{-1}$, reflecting typical cirrus cloud formation conditions, and water uptake and ice formation are recorded. Every 0.02 K, or 12 s, an image is taken providing time, substrate temperature, and dew point. This information is used to identify IMF and DIN modes and to derive heterogeneous ice nucleation rate coefficients, $J_{het}$, in units $cm^{-2}$ $s^{-1}$ and INAS density, $n_s$, in units $cm^{-2}$ following analyses described in detail previously (Alpert et al., 2022; Knopf et al., 2022; Knopf et al., 2020; Alpert et al., 2011b; Wang and Knopf, 2011; China et al., 2017). Only the first observed ice nucleation event is applied in the ice nucleation kinetics analysis since subsequent ice crystal formation can lead to an inhomogeneous field of humidity, rendering the $RH_{ice}$ value at which ice formed uncertain (Knopf, 2023).

Digital imaging analysis allows to relocation of the identified INP on the substrate in other micro-spectroscopic analytical instruments such as SEM/EDX (Knopf et al., 2022; Alpert et al., 2022; Knopf et al., 2014). Once ice formation is detected, ice sublimation under higher resolution (1130×) is performed as shown in Fig. S4a and b. The residual particle is identified as the INP. A sequence of optical microscope images showing different field of views are used to relocate the INP in other microscopic instruments by means of pattern recognition and triangulation. Figure S4c and d show a magnified field of view and the identified INP, respectively, using SEM.

## 3. Results and discussion

### 3.1 Particle population characterization

Figure 1 provides representative false-color particle population MS images and size-resolved MS and OVF analyses for MBL particle samples derived from STXM/NEXAFS analyses. S-MBL1 sample, collected during summer, shows a different particle population MS compared to the wintertime W-MBL1-DI and W-MBL2 samples. Additional particle population MS images are shown in Fig. S5 that corroborate this trend. Particles in the S-MBL1 sample are smaller and dominated by OCIN particles with few OC particles. W-MBL1-DI sample indicates the presence of OCIN particles with thick coatings of OC. This is also the case for sample W-MBL2, though particles seem to be larger, contain C=C double bonds, and generally appear to be chemically more complex. Size-resolved MS and OVF analyses for sample S-MBL1 indicate that OCIN particles dominate the population, with a significant fraction of IN particles in the smallest size range, and the majority of particles having an OVF between 20 and 60 %. The particle size distribution is unimodal with the largest particles smaller than 1 μm. MBL samples from collected during winter show a bimodal particle size distribution including particles with sizes up to 2 μm. Sample W-MBL1-DI is dominated by OCIN particles with OVFs between 20 to 60% while particles in sample W-MBL2 are more diverse and include EC and OC particles resulting in OVF ranging from 20 to 80 %.

Figure 1 and Fig. S5 demonstrate a difference in particle population MS between S- and W-MBL samples. We discuss potential factors that might explain the observed different particle population MS among MBL samples collected during different seasons. The Azores are located at the southern border of the North Atlantic storm tracks. While in summer surface winds can be calm, during winter, winds are generally higher (Laurila et al., 2021). Also during winter time, the occurrence of midlatitude DIs coinciding with the North Atlantic storm tracks is much more frequent (Raveh-Rubin, 2017). Ocean conditions such as water temperature and primary production as indicated by chlorophyll *a* concentrations are also different between summer and winter seasons. Figures S6 and S7 show Aqua MODIS (Moderate Resolution Imaging Spectroradiometer) derived monthly mean sea surface temperatures and chlorophyll *a* concentrations (Nasa Goddard Space Flight Center, 2019, 2022). During summer, ocean water in the ENA region is warmer and it has less biological production. During wintertime chlorophyll *a* concentrations in waters surrounding the Azores Islands are greater (Fig. S7). The ENA region also experiences greater wind speeds and more sustained winds during the winter generating more and larger SSA particles. These factors could impact primary marine organic emissions associated with SSA particles. Also, we have shown that during wintertime the Azores region is prone to DI events (Tomlin et al., 2021). As shown in Table 1, W-MBL1-DI and W-MBL2-DI samples were collected as Graciosa Island region experienced DI events. These DI events can significantly change the characteristics of the MBL particle population resulting in the presence of particles with complex composition (Tomlin et al., 2021). Greater wind speeds and primary productivity during winter may support the presence of larger INOC particles compared to the summer MBL sample while the mixing in of air masses from the upper troposphere from DIs may dilute the local MBL SSA particle population. Clearly, more samples and longer-term studies are needed to address those suggestions.

Representative false-color particle population MS images and size-resolved MS and OVF analyses for FT particle samples derived from STXM/NEXAFS analyses are shown in Figure 2. Images from sample S-FT1 display numerous submicron-sized particles dominated by OCIN particles with EC and IN particles contributing to those in the smaller sizes. The corresponding OVF ranges between 20 and 60 %. As in the case of the MBL samples, the S-FT1 sample collected during summer shows significantly different population characteristics compared to the wintertime collected FT samples. These differences are demonstrated further in Fig. S8. Backward trajectories suggest that air masses associated with S-FT1 remained for the most part over the Atlantic Ocean (Fig. S1) while W-FT1-DI and W-FT2 might have been impacted by air masses passing over the eastern continental north America (Fig. S3). Particles collected in sample W-FT3-DI appear to have originated solely from greater altitudes (Fig. S3). Particles in samples W-FT1-DI-3, W-FT2, and W-FT3-DI show greater MS diversity, include many in the larger size range, and the population includes particles with greater OVFs compared to sample S-FT1. OCIN particles still represent a major particle-type fraction but, specifically, for samples W-FT2 and W-FT3-DI, EC, OC, and IN particles, and mixtures thereof, also contribute significantly to the particle population. The sample W-FT3-DI, collected at the highest altitude of about 4056 m (Table 1), exhibits the highest OVFs, characterized by the largest contribution of purely OC particles compared to other samples. W-FT1-DI and W-FT3-DI samples experienced DI events that potentially impacted the particle population. Based on larger particle samples and application of CCSEM/EDX, Tomlin et al. (2021) observed that the relative carbonaceous contributions to the FT particle population decreases while the inorganic contribution increases during DI events. They also observed an increase in OVF for particle samples impacted by DIs. The FT samples are expected to be impacted by long-range transport, thus, physicochemical transformations by aging processes are expected (Tomlin et al., 2021; China et al., 2017; Lata et al., 2021). Hence, transport dynamics and DI events are likely impacting the FT particle population to a greater extent than changes in seawater characteristics resulting from seasonal differences in the abundances and activities of planktonic microorganisms.

Figure 3 presents OVF false color images and high resolution NEXAFS spectra representative of MBL and FT particle samples. The MBL samples are dominated by OCIN particle types which may reflect the island location and the fact that SSA particles from the marine environment consist of an inorganic core coated with varying amounts of organic material (Alpert et al., 2022; Laskin et al., 2016; Knopf et al., 2014; Pham et al., 2017; Ault et al., 2013b; Lee et al., 2020; Cochran et al., 2017). The NEXAFS spectra of the organic particle fraction presented in Fig. 3 shows the typical signatures of fresh and aged sea salt particles including the absorption bands of carboxyl and carbonate groups and the presence of potassium (Knopf et al., 2014; Alpert et al., 2022; Laskin et al., 2012; Knopf et al., 2022; Pham et al., 2017). In fact, the organic coating displays the same NEXAFS spectral features as SSA particles that have been demonstrated to serve as INPs (Alpert et al., 2022). As discussed in *Alpert et al.* (2022) the carbonate signal is due to beam damage with the conversion of the carboxyl group into a carbonate group. Detailed particle images in Fig. 3 show the distribution of identified particle species where OC, carbonate, and potassium are located on the outside of the particle.

In Fig. 3 it is apparent that particles collected in the FT have greater MS diversity, consistent with different NEXAFS spectral features. Included are particles dominated by elemental carbon signatures, aged sea salt particles, mineral rich

particles, and particle mixtures. Corresponding particle images display greater physicochemical complexity compared to MBL particles. These findings agree with the observations by *Tomlin et al.* (2021).

### 3.1 INP identification

Twelve INPs from the FT samples were identified and analyzed for their morphology and elemental composition using SEM/EDX. Figure 4 shows electron micrographs of INPs active in the DIN mode as well as associated observed ice formation temperatures. These INPs are categorized as sea salt, sea salt + sulfate, and OC particles based on their elemental composition (Table 3). The INP elemental compositions derived by SEM/EDX and corresponding EDX spectra are summarized in Fig. 5. Figures S9 and S10 provide more detailed EDX spectra and additional INP images. The INPs identified for these three different FT samples vary in composition (Table 3), although all of them have OM associated with them. Identified INPs from S-FT1 are comprised mostly of sea salt particles, though mineral dust and one unidentified particle type were also observed to act as INPs. INPs associated with W-FT1-DI display features of sea salt in the presences of sulfates, hinting at processed or aged particles. INPs from W-FT3-DI samples are purely carbonaceous in nature. No traces of other elements could be detected in those two INPs (Figs. 5 and S10). In this case, we can only speculate that these organic particles were likely in a glassy phase state when acting as INPs at -50 °C.

The FT INPs identified here are compared to INPs characterized from ground collected samples during the ACE-ENA campaign (Knopf et al., 2022). That study also identified sea salt, processed sea salt, and carbonaceous particles as INPs. INP measurements and identification at the Observatory of Mountain Pico site also observed aged sea salt, carbonaceous, and sulfate and carbonaceous coated dust particles which served as INPs (China et al., 2017; Lata et al., 2021). Overall, we find that the majority of identified INPs on all samples regardless of where collected belong to the major particle-types of the particle population and are not different or unique particles. This finding is consistent with similar findings from other field campaigns that have applied micro-spectroscopic analytical techniques to examine particle populations and identified INPs (Hiranuma et al., 2013; Knopf et al., 2022; China et al., 2017; Knopf et al., 2014; Lata et al., 2021).

### 3.2 Ice nucleation experiments

The ice nucleation experiments for the 7 particle samples are summarized in Fig. 6. Observed water uptake, IMF, and DIN events are plotted as a function of particle temperature and $RH_{ice}$. The S-MBL1 sample shows different ice nucleation propensity compared to the W-MBL-DI samples that were collected during DI events. ~~Water uptake occurs at lower $RH_{ice}$ compared to the IOP2 MBL samples.~~ Only for the S-MBL1 sample, IMF was observed at about 240 K below and at saturation indicating greater IMF propensity compared to W-MBL-DI samples. Also, IMF proceeded over a greater range of $RH_{ice}$ and at lower $RH_{ice}$ compared to W-MBL-DI samples. Lastly, DIN proceeds, on average, at lower $RH_{ice}$ compared to W-MBL-DI samples. Overall, these ice nucleation results reflect the above discussed differences in particle populations between the S-MBL1 and W-MBL-DI samples. Furthermore, it highlights the importance of DI events on the MBL particle populations and,

potentially, on INP sources. The role of DI events in changing the MS and OVF of the particle populations in the MBL and FT has been demonstrated by Tomlin et al. (2021).

Since the INPs are organic particles and/or are associated with OC coatings, Fig. 6 includes the glass transition temperatures, $T_g$, of several aerosol types for comparison, including SOA particles formed from the precursor gases α-pinene, naphthalene (Charnawskas et al., 2017) and ambient SOA and Suwannee river fulvic acid particles (Wang et al., 2012a). Also included is the full deliquescence relative humidity of SOA generated from α-pinene precursor gas, valid for the experimentally applied humidification rate (Charnawskas et al., 2017). DIN can proceed on glassy organic particles while IMF can proceed until the full deliquescence relative humidity is reached (Knopf et al., 2018). Once the particle is fully deliquesced, only homogeneous freezing can proceed when temperatures are sufficiently low (Berkemeier et al., 2014; Zobrist et al., 2008). Of these particle types, fulvic acid has the highest $T_g$ (Fig. 6), likely because it is a large macromolecule (Koop et al., 2011). SSA-INPs consist of polysaccharidic and proteinaceous macromolecular compounds (Alpert et al., 2022), which likely possess a high $T_g$ (Koop et al., 2011; Shiraiwa et al., 2011). DIN for MBL samples falls in the range of glassy fulvic acid particles. One can expect the full deliquescence relative humidity of fulvic acid to be significantly higher than for α-pinene derived SOA, possibly explaining the observed IMF for temperatures as high as 240 K in the case of S-MBL1 sample. This may point to the importance of glassy carbonaceous particles or particles coated by glassy OM to serve as INPs, although further microscopic investigations are necessary to confirm such a pathway. Figure 6 further includes the range of pore condensation freezing for pore sizes of 7.5 to 20 nm (Marcolli, 2020, 2014). Observed DIN events for S-MBL1 samples fall in this range of pore condensation freezing, however, for W-MBL1-DI and W-MBL2-DI observed ice formation falls mostly outside the pore condensation freezing active range of temperature and $RH_{ice}$.

As pointed out above, the STXM derived particle morphology and NEXAFS spectral features of the organic compounds associated with the particles in the MBL samples, are identical to the OM detected in SSA particles and SSA-INPs (Alpert et al., 2022). One would expect particles having similar physicochemical properties, similar ice nucleation characteristics with respect to the measured different nucleation pathways and thermodynamic conditions should be observed. Indeed, the range of water uptake, IMF, and DIN for S-MBL1 in Fig. 6 (not affected by DI events, but dominated by SSA emissions) match the conditions of SSA-INPs associated with various mesocosm experiments with marine microorganisms and field-collected particles (*Alpert et al.* (2022), their Fig. 1). These results further support the conclusions by *Alpert et al.* (2022) that "all SSA particles derived from aquatic environments regardless of the specific makeup of the planktonic community can serve as INPs because they contain the same ice-nucleating agents". It also demonstrates that if instrumentation which can resolve physicochemical properties on the nanoscale, e.g., the presence of the surface components, is available in combination with component-specific ice nucleation parameterizations, then atmospheric ice formation can be predicted (Knopf et al., 2021).

Compared to the MBL samples, FT samples show water uptake and DIN at lower $RH_{ice}$ (Fig. 6). Particles in sample S-FT1 which were not affected by DI, and particles in W-FT3-DI which were collected at 4000 m, the highest altitude, show IMF at the highest temperatures of about 240 K. IMF for W-FT2 and W-FT3-DI samples proceeds only at about 230 K.

Overall, FT samples demonstrate greater ice nucleation propensity compared to the MBL samples, while S-FT1 shows the greatest ice nucleation efficiency among all samples.

Previous INP measurements at the Observatory of Mountain Pico that typically resides in the free troposphere (China et al., 2017; Lata et al., 2021) show DIN and IMF conditions similar to the FT samples investigated here. *Lata et al.* (2021) have shown that FT samples include solid organic particles that are likely responsible for DIN. The example $T_g$ and full deliquescence relative humidity curves shown in Fig. 6 suggest that DIN and IMF proceeded on highly viscous or solid particles. Clearly, these collective observations emphasize the need for a better understanding of how highly viscous OC species interact with water initiating ice nucleation.

### 3.2 Immersion freezing kinetics

IMF rates are expressed by $J_{\mathrm{het}}$ and $n_{\mathrm{s}}$ (Knopf et al., 2022; China et al., 2017; Alpert et al., 2011b). We apply ABIFM (Knopf and Alpert, 2013) to parameterize $J_{\mathrm{het}}$ and $n_{\mathrm{s}}$ as a function of the water activity criterion, $\Delta a_w$, where $\Delta a_w(T) = a_w(T) - a_w^i(T)$ (Koop et al., 2000). A necessary condition for the application of $\Delta a_w$ is that condensed-phase water activity, $a_w$, is in equilibrium with adjacent water partial pressure, resulting in $a_w = \mathrm{RH}$. $a_w^i(T)$ is the ice melting curve for frozen aqueous solutions as a function of water activity (Koop and Zobrist, 2009). Application of ABIFM allows the expression of heterogeneous freezing kinetics as a function of temperature and RH with a single parameter, thereby also covering the subsaturated temperature range (Knopf and Alpert, 2023). $\Delta a_w = 0$ represents the melting point of ice at 273.15 K and $\Delta a_w = 0.313$ represents the homogeneous ice nucleation temperature at 238 K and $J_{\mathrm{hom}} \sim 10^{10}$ cm$^{-3}$ s$^{-1}$ (Koop et al., 2000).

Figure 7 shows derived IMF $J_{\mathrm{het}}$ and $n_{\mathrm{s}}$ values as a function of $\Delta a_w$, for MBL and FT samples. With increasing $\Delta a_w$ $J_{\mathrm{het}}$ and $n_{\mathrm{s}}$ are increasing. For MBL samples, average $J_{\mathrm{het}} \sim 200$ cm$^{-2}$ s$^{-1}$ and $n_{\mathrm{s}} \sim 2000$ cm$^{-2}$. A recent study by *Cornwell et al.* (2021) derived $J_{\mathrm{het}}$(243 K) ~ 1000 cm$^{-2}$ s$^{-1}$ corresponding to $\Delta a_w \sim 0.25$, about a factor of three greater than our derived $J_{\mathrm{het}}$ values but still within the uncertainties of both measurements. The $n_{\mathrm{s}}$ values at 243 K agree with previous laboratory and field measurements of SSA and MBL field collected particles reported by *McCluskey et al.* (2017) and *DeMott et al.* (2016). FT samples show a trend of greater $J_{\mathrm{het}}$ and $n_{\mathrm{s}}$ values with average $J_{\mathrm{het}} \sim 700$ cm$^{-2}$ s$^{-1}$ and $n_{\mathrm{s}} \sim 8000$ cm$^{-2}$ compared to MBL samples. Though this trend is within the stated uncertainties of $J_{\mathrm{het}}$ and $n_{\mathrm{s}}$. For the MBL samples, $J_{\mathrm{het}}$ and $n_{\mathrm{s}}$ data are expressed by a linear regression following ABIFM, where $\log J_{\mathrm{het}} = ma_w + c$ and $\log n_{\mathrm{s}} = ma_w + c$, respectively and the fit parameters and associated uncertainties are given in Table 4. Since IMF FT data do not show a clear trend with $\Delta a_w$ no linear regression is provided. A possible reason for the greater scatter in FT $J_{\mathrm{het}}$ and $n_{\mathrm{s}}$ may be the greater chemical diversity and complexity of the particles present in these samples.

When comparing derived IMF $J_{\mathrm{het}}$ with $J_{\mathrm{het}}$ for illite (Knopf and Alpert, 2013), natural mineral dust (Alpert and Knopf, 2016; Niemand et al., 2012), leonardite, a humic acid (Rigg et al., 2013; Knopf and Alpert, 2013), and diatomaceous material (Knopf and Alpert, 2013; Knopf et al., 2011; Alpert et al., 2011a; Alpert et al., 2011b), the field derived $J_{\mathrm{het}}$ values show a shallower slope, and therefore greater $J_{\mathrm{het}}$ at lower $\Delta a_w$ (i.e., higher temperature) and lower $J_{\mathrm{het}}$ at larger $\Delta a_w$ (i.e.,

lower temperature). In Fig. 7, we also included a recently derived ABIFM IMF $J_{het}$ parameterization for SSA which act as INPs (Alpert et al., 2022). Since the observed ice formation conditions and particle composition are similar to the SSA studied in *Alpert et al.* (2022), similar $J_{het}$ values are expected. However, this parameterization also displays a greater slope with $\Delta a_w$ compared to the field derived IMF $J_{het}$. The most likely explanation for this difference lies in the IMF analysis itself. *Alpert et al.* (2022) analyzed the IMF data of several data sets with a stochastic freezing model that accounts for particle surface area uncertainties. As shown in *Alpert and Knopf* (2016), the inclusion of particle surface area uncertainty produces a steeper slope of IMF $J_{het}$, compared to the one when assuming that all particles possess the same surface area. This can amount to differences in $J_{het}$ at the lower and higher temperatures of several orders of magnitude (Alpert and Knopf, 2016). Accounting of particle surface uncertainty, however, has not been performed for these field derived data and are beyond the scope of this study.

The ABIFM IMF $J_{het}$ parameterization derived from ground site measurements during ACE-ENA (Knopf et al., 2022) agree with the IMF $J_{het}$ derived for MBL samples (Fig. 7). Although the ground measurements were based on samples with different particle loading and different INP sizes, the IMF kinetics are very similar when accounting for particle surface area. This finding supports the usefulness of ground site INP measurements in a well-mixed MBL. ABIFM IMF $J_{het}$ parameterization derived from particle samples collected at Observatory of Mountain Pico are also plotted in Fig. 7. Recent measurements by *Lata et al.* (2021) demonstrate better agreement with airborne derived IMF $J_{het}$ compared to IMF $J_{het}$ derived by China et al. (2017), though, when considering uncertainties, all parameterizations show significant overlap.

### 3.3 Deposition ice nucleation kinetics.

We first analyzed DIN kinetics following CNT expressed using the contact angle, $\theta$ (Knopf et al., 2022; Alpert et al., 2011b; Wang and Knopf, 2011). A smaller $\theta$ value indicates greater ice nucleation propensity while $\theta$ = 180° corresponds to the case of homogeneous ice nucleation (Knopf et al., 2022; Pruppacher and Klett, 1997; Zobrist et al., 2007). Figure 8a shows $J_{het}$ as a function of temperature where FT samples demonstrate DIN at higher temperatures compared to MBL samples. Typical $J_{het}$ values are in the range of 1000 cm$^{-2}$ s$^{-1}$. Corresponding $\theta$ values are given in Fig. 8b where, at similar temperatures, greater $J_{het}$ values correspond to smaller $\theta$ values. $\theta$ values for the MBL samples are distributed around 25°. This $\theta$ value is in the range of $\theta$ values observed for carbonaceous laboratory-generated and field-collected particles while mineral dust particles typically exert smaller $\theta$ values (Wang et al., 2012a). FT samples are associated with $\theta$ values as low as 15°, implying superior DIN compared to the MBL samples. This may be due to the presence of inorganic species such as mineral dust. Figure 8c depicts derived $\theta$ values as a function of $RH_{ice}$. This analysis reflects the fact that DIN on the FT samples is superior to DIN proceeding on the MBL samples. Overall, the derived $\theta$ values follow the suggested DIN parameterization by *Wang and Knopf* (2011).

We also analyzed DIN applying $\Delta a_w$ (Knopf et al., 2022; China et al., 2017) as shown in Fig. 9 generating DIN $J_{het}$ and $n_s$ values for examined MBL and FT samples. With increasing $\Delta a_w$ $J_{het}$ and $n_s$ are continuously increasing. For MBL and FT samples, DIN $J_{het}$ ~ 550 cm$^{-2}$ s$^{-1}$ and $n_s$ ~ 7500 cm$^{-2}$, although ice nucleation occurs at lower $\Delta a_w$ for FT samples

indicating greater DIN propensity compared to MBL samples. ~~Hence,~~ Compared to the IMF case, a clearer difference between MBL and FT samples is visible. DIN $J_{het}$ and $n_s$ for FT samples display a steeper slope than for MBL samples.~~, having greater $J_{het}$ and $n_s$ values at $\Delta a_w \sim 0.2$.~~ We expressed $J_{het}$ and $n_s$ data for MBL and FT samples by linear regressions following ABIFM with the fit parameters given in Table 4. We compare these two DIN parameterizations with the one derived at the ground site at ACE-ENA during similar time periods (Knopf et al., 2022). The ground-site derived DIN parameterization falls in between the MBL and FT DIN parameterization, though considering the uncertainties, it is not significantly different compared to the parameterizations based on airborne-collected data. We also plotted a recent DIN parameterization for SSA particles (Alpert et al., 2022). Within stated uncertainties, values of $J_{het}$ for SSA particles agree with the newly derived DIN parameterizations while it more closely represents the MBL samples.

## 4. Atmospheric implications

The results of this study clearly demonstrate that the sampling season, DI events, and sampling altitude, specifically MBL versus FT regions, can impact the makeup of the particle population and as such the INPs and their freezing potential. Wintertime MBL samples impacted by DI events show the greatest contrast in terms of particle population and freezing characteristics with summertime MBL samples in the absence of DI events. FT samples show greater diversity in the physicochemical makeup of the particle population and, for the most part, demonstrate greater ice nucleation propensity. These findings complicate the designation of INP sources when modeling cloud formation. In the study area, DI events which were most frequent during wintertime, have the greatest impact on the particle and INP population. For a well-mixed MBL as encountered in this study, MBL INP parameterizations derived from ground site measurements agree with the airborne derived INP parameterizations. However, application of ground-site derived INP parameterizations may not always be suitable for predicting INP number concentrations in the FT, although differences can lie within the uncertainties of those parameterizations.

Most of the identified INPs reflect particle-types that are abundant in the particle population. This study corroborates the ice formation potential of SSA particles (Alpert et al., 2022; McCluskey et al., 2018; DeMott et al., 2016; Cornwell et al., 2021; Knopf et al., 2022), mineral dust particles (Kanji et al., 2017), and organic particles (Knopf et al., 2018). In the presence of these particle types in the MBL and FT, derived IMF and DIN INP parameterization allow for estimation of INP number concentrations. The developed IMF and DIN parameterizations are based on $\Delta a_w$, which allows for a computationally efficient implementation in cloud and climate models while using the same framework as for homogeneous ice nucleation (Alpert et al., 2022; Knopf and Alpert, 2023). This in turn allows for a complete description of IMF, DIN, and homogeneous ice nucleation based on the same parameter space, again facilitating computational application.

## 5. Conclusions

The population composition, INP morphology and composition, IMF and DIN conditions and associated freezing kinetics of particles in the MBL and FT in the Azores Islands region collected during the ACE-ENA campaign during summer and winter show distinct differences. Micro-spectroscopic single-particle analysis by STXM/NEXAFS indicates that the physicochemical properties of the particle population differ among the summer and winter samples and when DI events prevailed. The latter corroborates the findings by *Tomlin et al.* (2021). These differences are also reflected in the conditions under which IMF and DIN were observed for the examined particles. In general, particles collected in the FT show greater morphological and chemical complexity compared to MBL particles which highlights the importance of long-range transport, chemical transformation, and different particle sources which can impact the local particle population. MBL particles were dominated by inorganic-organic mixtures that reflect the ocean influence with SSA particles having the same composition and absorption spectral features as SSA particles and INPs described in previous studies (Alpert et al., 2022; Knopf et al., 2022). We can conclude that for the Azores Island region, seasonal changes and sampling altitude affect the particle population characteristics and as such the INP sources.

INP identifications using SEM/EDX show that most of the INPs are sea salt, sea salt with sulfate, dust, and carbonaceous particles, all of which are associated with OM. Given that these particle types are also present in the general particle population of the samples, they are not unique, at least at the nanometer-scale resolution of the micro-spectroscopic single particle techniques used. This conclusion is similar to that of other studies that have used micro-spectroscopic single particle analytical techniques to examined particle populations and associated INPs or ice crystal residues (Alpert et al., 2022; Knopf et al., 2022; China et al., 2017; Knopf et al., 2014; Lata et al., 2021; Hiranuma et al., 2013). These observations further emphasize the importance of organic compounds for ice nucleation and suggest the necessity of a better molecular understanding of the species involved and their phase state in response to ambient temperature and humidity.

The particles in both MBL and FT samples displayed different conditions with respect to temperature and $RH_{ice}$ for initiating water uptake, IMF, and DIN. MBL particles that experienced DI showed greater susceptibility for water uptake, did not initiate IMF at ~240 K, and displayed less efficient DIN compared to particles collected in the MBL during summertime when there were no DI events. The summertime FT particles, however, displayed different conditions for initiating water uptake, IMF, and DIN compared to the wintertime samples. FT particle samples, in general, were found to have greater ice nucleation propensity compared to the MBL samples. The reason for these differences may lie in differences in particle composition and chemical transformation during long-range transport (Li and Knopf, 2021; China et al., 2017).

IMF freezing efficiencies, expressed in $J_{\mathrm{het}}$ and $n_{\mathrm{s}}$ values were derived following ABIFM. MBL IMF in $J_{\mathrm{het}}$ and $n_{\mathrm{s}}$ can be expressed by a log-linear regression and agrees with an IMF ABIFM parameterization derived from ACE-ENA ground site measurements (Knopf et al., 2022). This implies that in the well-mixed MBL encountered during ACE-ENA and when accounting for particle number concentration and surface area, airborne and ground sampling of INPs can produce similar freezing kinetics. DIN analyzed in terms of CNT, derives the contact angle from $J_{\mathrm{het}}$ as a function of temperature and $RH_{ice}$

and results followed the DIN parameterization given by *Wang and Knopf* (2011). DIN is also expressed as a function of the water activity criterion, $\Delta a_w$, resulting in a log-linear regression of $J_{\text{het}}$ and $n_s$ values as a function of $\Delta a_w$. DIN parameterization for FT particle samples shows greater ice nucleation propensity compared to MBL particle samples.

The differences in the IMF and DIN kinetics analyses reflect the differences in the particle population which, in this study depended on the seasonal sampling period and sampling height. The unique opportunity to collect particles in the MBL and FT during different seasons allowed us to examine the corresponding particle populations and INPs. This study emphasizes the importance of INP measurements that cover seasonal changes and a range of altitudes. For a well-mixed MBL, INP measurements at ground level and airborne may result in similar data. Hence, for mixed-phase clouds that form within the well-mixed MBL, which includes certain types of Arctic mixed-phase clouds, ground site INP measurements may suffice for particle characterization. However, in lower latitudes where the ice melting line is above the MBL, additional sampling of INPs aloft would be preferential to better establish the INP sources.

**Data availability.** All data needed to draw the conclusions in the present study are given in the paper or in the Supplement.

**Supplement.** The supplement related to this article is available online at:

**Author contributions.** DAK envisioned and supervised the project, performed STXM/NEXAFS experiments and analysis, conducted ice nucleation analyses, and wrote the first draft of the manuscript. PW conducted ice nucleation experiments and assisted in STXM/NEXAFS experiments. BW, AL, JMT, RCM, JYA, MAM assisted in STXM/NEXAFS experiments and analyses. DPV, NNL, SC, conducted SEM/EDX experiments and analyses. JW oversaw aircraft deployment and particle collection. All authors discussed interpretation of the data and contributed to the writing of the manuscript.

**Competing interests.** Some of the authors are members of the editorial board of Atmospheric Chemistry and Physics. The peer review process was guided by an independent editor. The authors have no other competing interests to declare.

**Acknowledgements.** This study was supported by the Atmospheric System Research Program and Atmospheric Radiation Measurement Program sponsored by the U.S. Department of Energy (DOE), Office of Science, Office of Biological and Environmental Research (OBER), Climate and Environmental Sciences Division (CESD). DAK acknowledges support by the U.S. DOE grants DE-SC0016370 and DE-SC0021034. RCM and AL acknowledge by the U.S. DOE grant DE-SC0021977. JW acknowledges funding support from the US DOE grants DE-SC0020259 and DE-SC0021017. A portion of this research was performed on a project award (10.46936/lser.proj.2019.50738/60000088 and 10.46936/sthm.proj.2017.49857/60006200) from the Environmental Molecular Sciences Laboratory, a DOE Office of Science User Facility sponsored by the Biological and Environmental Research program under Contract No. DE-AC05-76RL01830. The STXM/NEXAFS particle analysis was performed at beamlines 5.3.2.2 and 11.0.2 at the Advanced Light Source (ALS) at Lawrence Berkeley National Laboratory.

The work at the ALS was supported by the Director, Office of Science, Office of Basic Energy Sciences, of the U.S. DOE under contract DE-AC02-05CH11231.

**Financial support**. This research has been supported by the U.S. Department of Energy (grant nos. DE-SC0016370, DE-SC0021034, DE-SC0021977, DE-SC0020259, DE-SC0021017, DE-AC05-76RL01830, DE-AC02-05CH11231).

## References

Aller, J. Y., Radway, J. C., Kilthau, W. P., Bothe, D. W., Wilson, T. W., Vaillancourt, R. D., Quinn, P. K., Coffman, D. J., Murray, B. J., and Knopf, D. A.: Size-resolved characterization of the polysaccharidic and proteinaceous components of sea spray aerosol, Atmos. Environ., 154, 331-347, 10.1016/j.atmosenv.2017.01.053, 2017.

Alonso-Perez, S., Cuevas, E., Querol, X., Guerra, J. C., and Perez, C.: African dust source regions for observed dust outbreaks over the Subtropical Eastern North Atlantic region, above 25 degrees N, J. Arid. Environ., 78, 100-109, 10.1016/j.jaridenv.2011.11.013, 2012.

Alpert, P. A. and Knopf, D. A.: Analysis of isothermal and cooling-rate-dependent immersion freezing by a unifying stochastic ice nucleation model, Atmos. Chem. Phys., 16, 2083-2107, 10.5194/acp-16-2083-2016, 2016.

Alpert, P. A., Aller, J. Y., and Knopf, D. A.: Ice nucleation from aqueous NaCl droplets with and without marine diatoms, Atmos. Chem. Phys., 11, 5539–5555, 10.5194/acp-11-5539-2011, 2011a.

Alpert, P. A., Aller, J. Y., and Knopf, D. A.: Initiation of the ice phase by marine biogenic surfaces in supersaturated gas and supercooled aqueous phases, Phys. Chem. Chem. Phys., 13, 19882-19894, 10.1039/C1CP21844A, 2011b.

Alpert, P. A., Kilthau, W. P., Bothe, D. W., Radway, J. C., Aller, J. Y., and Knopf, D. A.: The influence of marine microbial activities on aerosol production: A laboratory mesocosm study, J. Geophys. Res.-Atmospheres, 120, 8841-8860, 10.1002/2015jd023469, 2015.

Alpert, P. A., Kilthau, W. P., O'Brien, R. E., Moffet, R. C., Gilles, M. K., Wang, B., Laskin, A., Aller, J. Y., and Knopf, D. A.: Ice-nucleating agents in sea spray aerosol identified and quantified with a holistic multi-modal freezing model, Sci. Adv., 8, eabq6842, 10.1126/sciadv.abq6842, 2022.

Ault, A. P., Moffet, R. C., Baltrusaitis, J., Collins, D. B., Ruppel, M. J., Cuadra-Rodriguez, L. A., Zhao, D., Guasco, T. L., Ebben, C. J., Geiger, F. M., Bertram, T. H., Prather, K. A., and Grassian, V. H.: Size-Dependent Changes in Sea Spray Aerosol Composition and Properties with Different Seawater Conditions, Environ. Sci. Technol., 47, 5603-5612, 10.1021/es400416g, 2013a.

Ault, A. P., Moffet, R. C., Baltrusaitis, J., Collins, D. B., Ruppel, M. J., Cuadra-Rodriguez, L. A., Zhao, D. F., Guasco, T. L., Ebben, C. J., Geiger, F. M., Bertram, T. H., Prather, K. A., and Grassian, V. H.: Size-Dependent Changes in Sea Spray Aerosol Composition and Properties with Different Seawater Conditions, Environ. Sci. Technol., 47, 5603-5612, 10.1021/es400416g, 2013b.

Baker, M. B.: Cloud microphysics and climate, Science, 276, 1072-1078, 1997.

Berkemeier, T., Shiraiwa, M., Pöschl, U., and Koop, T.: Competition between water uptake and ice nucleation by glassy organic aerosol particles, Atmos. Chem. Phys., 14, 12513-12531, 10.5194/acp-14-12513-2014, 2014.

Boucher, O., Randall, D., Artaxo, P., Bretherton, C., Feingold, G., Forster, P., Kerminen, V.-M., Kondo, Y., Liao, H., Lohmann, U., Rasch, P., Satheesh, S. K., Sherwood, S., Stevens, B., and Zhang, X. Y.: Clouds and Aerosols, in: Climate Change 2013: The Physical Science Basis. Contribution of Working Group I to the Fifth Assessment Report of the Intergovernmental Panel on Climate Change, edited by: Stocker, T. F., Qin, D., Plattner, G.-K., Tignor, M., Allen, S. K., Boschung, J., Nauels, A., Xia, Y., Bex, V., and Midgley, P. M., Cambridge University Press, Cambridge, United Kingdom and New York, NY, USA, 2013.

Cantrell, W. and Heymsfield, A.: Production of ice in tropospheric clouds - A review, Bull. Amer. Meteorol. Soc., 86, 795-807, 10.1175/bams-86-6-795, 2005.

Charnawskas, J. C., Alpert, P. A., Lambe, A. T., Berkemeier, T., O'Brien, R. E., Massoli, P., Onasch, T. B., Shiraiwa, M., Moffet, R. C., Gilles, M. K., Davidovits, P., Worsnop, D. R., and Knopf, D. A.: Condensed-phase biogenic-anthropogenic interactions with implications for cold cloud formation, Faraday Discuss., 200, 164-195, 10.1039/C7FD00010C, 2017.

China, S., Alpert, P. A., Zhang, B., Schum, S., Dzepina, K., Wright, K., Owen, R. C., Fialho, P., Mazzoleni, L. R., Mazzoleni, C., and Knopf, D. A.: Ice cloud formation potential by free tropospheric particles from long-range transport over the Northern Atlantic Ocean, J. Geophys. Res., 122, 3065-3079, 10.1002/2016jd025817, 2017.

Cochran, R. E., Ryder, O. S., Grassian, V. H., and Prather, K. A.: Sea Spray Aerosol: The Chemical Link between the Oceans, Atmosphere, and Climate, Accounts Chem. Res., 50, 599-604, 10.1021/acs.accounts.6b00603, 2017.

Connolly, P. J., Möhler, O., Field, P. R., Saathoff, H., Burgess, R., Choularton, T., and Gallagher, M.: Studies of heterogeneous freezing by three different desert dust samples, Atmos. Chem. Phys., 9, 2805-2824, 10.5194/acp-9-2805-2009, 2009.

Cornwell, G. C., McCluskey, C. S., DeMott, P. J., Prather, K. A., and Burrows, S. M.: Development of Heterogeneous Ice Nucleation Rate Coefficient Parameterizations From Ambient Measurements, Geophys. Res. Lett., 48, 10, 10.1029/2021gl095359, 2021.

Cornwell, G. C., McCluskey, C. S., Levin, E. J. T., Suski, K. J., DeMott, P. J., Kreidenweis, S. M., and Prather, K. A.: Direct Online Mass Spectrometry Measurements of Ice Nucleating Particles at a California Coastal Site, J. Geophys. Res.-Atmos., 124, 12157-12172, 10.1029/2019jd030466, 2019.

Creamean, J. M., Hill, T. C. J., DeMott, P. J., Uetake, J., Kreidenweis, S., and Douglas, T. A.: Thawing permafrost: an overlooked source of seeds for Arctic cloud formation, Environmental Research Letters, 15, 9, 10.1088/1748-9326/ab87d3, 2020.

Creamean, J. M., Cross, J. N., Pickart, R., McRaven, L., Lin, P., Pacini, A., Hanlon, R., Schmale, D. G., Ceniceros, J., Aydell, T., Colombi, N., Bolger, E., and DeMott, P. J.: Ice Nucleating Particles Carried From Below a Phytoplankton Bloom to the Arctic Atmosphere, Geophys. Res. Lett., 46, 8572-8581, 10.1029/2019gl083039, 2019.

Cziczo, D. J., Ladino, L. A., Boose, Y., Kanji, Z. A., Kupiskewski, P., Lance, S., Mertes, S., and Wex, H.: Measurements of Ice Nucleating Particles and Ice Residuals, Meteorological Monographs, 58, 8.1-8.13, 10.1175/amsmonographs-d-16-0008.1, 2017a.

Cziczo, D. J., Ladino, L. A., Boose, Y., Kanji, Z. A., Kupiszewski, P., Lance, S., Mertes, S., and Wex, H.: Measurements of Ice Nucleating Particles and Ice Residuals, in: Ice Formation and Evolution in Clouds and Precipitation: Measurement and Modeling Challenges, American Meteorological Society, 8.1-8.13, 10.1175/AMSMONOGRAPHS-D-16-0008.1, 2017b.

David, R. O., Marcolli, C., Fahrni, J., Qiu, Y., Perez Sirkin, Y. A., Molinero, V., Mahrt, F., Brühwiler, D., Lohmann, U., and Kanji, Z. A.: Pore condensation and freezing is responsible for ice formation below water saturation for porous particles, 10.1073/pnas.1813647116, 2019.

DeMott, P. J., Prenni, A. J., Liu, X., Kreidenweis, S. M., Petters, M. D., Twohy, C. H., Richardson, M. S., Eidhammer, T., and Rogers, D. C.: Predicting global atmospheric ice nuclei distributions and their impacts on climate, Proc. Natl. Acad. Sci. U. S. A., 107, 11217-11222, 10.1073/pnas.0910818107, 2010.

DeMott, P. J., Hill, T. C. J., McCluskey, C. S., Prather, K. A., Collins, D. B., Sullivan, R. C., Ruppel, M. J., Mason, R. H., Irish, V. E., Lee, T., Hwang, C. Y., Rhee, T. S., Snider, J. R., McMeeking, G. R., Dhaniyala, S., Lewis, E. R., Wentzell, J. J. B., Abbatt, J., Lee, C., Sultana, C. M., Ault, A. P., Axson, J. L., Martinez, M. D., Venero, I., Santos-Figueroa, G., Stokes, M. D., Deane, G. B., Mayol-Bracero, O. L., Grassian, V. H., Bertram, T. H., Bertram, A. K., Moffett, B. F., and Franc, G. D.: Sea spray aerosol as a unique source of ice nucleating particles, Proc. Natl. Acad. Sci. U. S. A., 113, 5797-5803, 10.1073/pnas.1514034112, 2016.

Facchini, M. C. and O'Dowd, C. D.: Biogenic origin of primary and secondary organic components in marine aerosol, Geochim. Cosmochim. Ac., 73, A348-A348, 2009.

Fraund, M., Park, T., Yao, L., Bonanno, D., Pham, D. Q., and Moffet, R. C.: Quantitative capabilities of STXM to measure spatially resolved organic volume fractions of mixed organic / inorganic particles, Atmos. Meas. Tech., 12, 1619-1633, 10.5194/amt-12-1619-2019, 2019.

Fraund, M., Bonanno, D. J., China, S., Pham, D. Q., Veghte, D., Weis, J., Kulkarni, G., Teske, K., Gilles, M. K., Laskin, A., and Moffet, R. C.: Optical properties and composition of viscous organic particles found in the Southern Great Plains, Atmos. Chem. Phys., 20, 11593-11606, 10.5194/acp-20-11593-2020, 2020.

Hill, T. C. J., DeMott, P. J., Tobo, Y., Fröhlich-Nowoisky, J., Moffett, B. F., Franc, G. D., and Kreidenweis, S. M.: Sources of organic ice nucleating particles in soils, Atmos. Chem. Phys., 16, 7195-7211, 10.5194/acp-16-7195-2016, 2016.

Hiranuma, N., Brooks, S. D., Moffet, R. C., Glen, A., Laskin, A., Gilles, M. K., Liu, P., Macdonald, A. M., Strapp, J. W., and McFarquhar, G. M.: Chemical characterization of individual particles and residuals of cloud droplets and ice crystals collected on board research aircraft in the ISDAC 2008 study, J. Geophys. Res., 118, 6564-6579, 10.1002/jgrd.50484, 2013.

Hopkins, R. J., Tivanski, A. V., Marten, B. D., and Gilles, M. K.: Chemical bonding and structure of black carbon reference materials and individual carbonaceous atmospheric aerosols, J. Aerosol Sci., 38, 573-591, 10.1016/j.jaerosci.2007.03.009, 2007.

Ilotoviz, E., Ghate, V. P., and Raveh-Rubin, S.: The Impact of Slantwise Descending Dry Intrusions on the Marine Boundary Layer and Air-Sea Interface Over the ARM Eastern North Atlantic Site, J. Geophys. Res.-Atmos., 126, 24, 10.1029/2020jd033879, 2021.

Irish, V. E., Hanna, S. J., Willis, M. D., China, S., Thomas, J. L., Wentzell, J. J. B., Cirisan, A., Si, M., Leaitch, W. R., Murphy, J. G., Abbatt, J. P. D., Laskin, A., Girard, E., and Bertram, A. K.: Ice nucleating particles in the marine boundary layer in the Canadian Arctic during summer 2014, Atmos. Chem. Phys., 19, 1027-1039, 10.5194/acp-19-1027-2019, 2019.

Kanji, Z. A., Ladino, L. A., Wex, H., Boose, Y., Burkert-Kohn, M., Cziczo, D. J., and Krämer, M.: Overview of Ice Nucleating Particles, in: Ice Formation and Evolution in Clouds and Precipitation: Measurement and Modeling Challenges, Meteorological Monographs, American Meteorological Society, 1.1-1.33, DOI: 10.1175/AMSMONOGRAPHS-D-16-0006.1, 2017.

Kilcoyne, A. L. D., Tyliszczak, T., Steele, W. F., Fakra, S., Hitchcock, P., Franck, K., Anderson, E., Harteneck, B., Rightor, E. G., Mitchell, G. E., Hitchcock, A. P., Yang, L., Warwick, T., and Ade, H.: Interferometer-controlled scanning transmission X-ray microscopes at the Advanced Light Source, J. Synchrotron Radiat., 10, 125-136, 2003.

Knopf, D. A.: Microanalysis Techniques to Study Atmospheric Ice Nucleation and Ice Crystal Growth, in: Microanalysis and Atmospheric Particles: Techniques and Applications in Climate Change and Air Quality, edited by: Conny, J. M., John Wiley & Sons, Hoboken, NJ, accepted, 2023.

Knopf, D. A. and Alpert, P. A.: A water activity based model of heterogeneous ice nucleation kinetics for freezing of water and aqueous solution droplets, Faraday Discuss., 165, 513-534, 10.1039/C3FD00035D, 2013.

Knopf, D. A. and Alpert, P. A.: Atmospheric ice nucleation, Nat. Rev. Phys., 10.1038/s42254-023-00570-7, 2023.

Knopf, D. A., Alpert, P. A., and Wang, B.: The Role of Organic Aerosol in Atmospheric Ice Nucleation: A Review, ACS Earth Space Chem., 2, 168–202, 10.1021/acsearthspacechem.7b00120, 2018.

Knopf, D. A., Alpert, P. A., Wang, B., and Aller, J. Y.: Stimulation of ice nucleation by marine diatoms, Nat. Geosci., 4, 88-90, 10.1038/ngeo1037, 2011.
Knopf, D. A., Alpert, P. A., Zipori, A., Reicher, N., and Rudich, Y.: Stochastic nucleation processes and substrate abundance explain time-dependent freezing in supercooled droplets, npj Clim. Atmos. Sci., 3, 1-9, 10.1038/s41612-020-0106-4, 2020.
Knopf, D. A., Wang, B., Laskin, A., Moffet, R. C., and Gilles, M. K.: Heterogeneous nucleation of ice on anthropogenic organic particles collected in Mexico City, Geophys. Res. Lett., 37, L11803, 10.1029/2010GL043362, 2010.
Knopf, D. A., Alpert, P. A., Wang, B., O'Brien, R. E., Kelly, S. T., Laskin, A., Gilles, M. K., and Moffet, R. C.: Microspectroscopic imaging and characterization of individually identified ice nucleating particles from a case field study, J. Geophys. Res., 119, 10365-10381, 10.1002/2014JD021866, 2014.
Knopf, D. A., Charnawskas, J. C., Wang, P. W., Wong, B., Tomlin, J. M., Jankowski, K. A., Fraund, M., Veghte, D. P., China, S., Laskin, A., Moffet, R. C., Gilles, M. K., Aller, J. Y., Marcus, M. A., Raveh-Rubin, S., and Wang, J.: Micro-spectroscopic and freezing characterization of ice-nucleating particles collected in the marine boundary layer in the eastern North Atlantic, Atmos. Chem. Phys., 22, 5377-5398, 10.5194/acp-22-5377-2022, 2022.
Knopf, D. A., Barry, K. R., Brubaker, T. A., Jahl, L. G., Jankowski, K. A., Li, J., Lu, Y., Monroe, L. W., Moore, K. A., Rivera-Adorno, F. A., Sauceda, K. A., Shi, Y., Tomlin, J. M., Vepuri, H. S. K., Wang, P., Lata, N. N., Levin, E. J. T., Creamean, J. M., Hill, T. C. J., China, S., Alpert, P. A., Moffet, R. C., Hiranuma, N., Sullivan, R. C., Fridlind, A. M., West, M., Laskin, A., DeMott, P. J., and Liu, X.: Aerosol–Ice Formation Closure: A Southern Great Plains Field Campaign, B. Am. Meteorol. Soc., 102, E1952–E1971 10.1175/BAMS-D-20-0151.1, 2021.
Koop, T.: Homogeneous ice nucleation in water and aqueous solutions, Z. Phys. Chemie-Int. J. Res. Phys. Chem. Chem. Phys., 218, 1231-1258, 2004.
Koop, T. and Zobrist, B.: Parameterizations for ice nucleation in biological and atmospheric systems, Phys. Chem. Chem. Phys., 11, 10839-10850, Doi 10.1039/B914289d, 2009.
Koop, T., Bookhold, J., Shiraiwa, M., and Pöschl, U.: Glass transition and phase state of organic compounds: dependency on molecular properties and implications for secondary organic aerosols in the atmosphere, Phys. Chem. Chem. Phys., 13, 19238-19255, 10.1039/c1cp22617g, 2011.
Koop, T., Luo, B. P., Tsias, A., and Peter, T.: Water activity as the determinant for homogeneous ice nucleation in aqueous solutions, Nature, 406, 611-614, 10.1038/35020537, 2000.
Ladino, L. A., Yakobi-Hancock, J. D., Kilthau, W. P., Mason, R. H., Si, M., Li, J., Miller, L. A., Schiller, C. L., Huffman, J. A., Aller, J. Y., Knopf, D. A., Bertram, A. K., and Abbatt, J. P. D.: Addressing the ice nucleating abilities of marine aerosol: A combination of deposition mode laboratory and field measurements, Atmos. Environ., 132, 1-10, 10.1016/j.atmosenv.2016.02.028, 2016.
Laskin, A., Cowin, J. P., and Iedema, M. J.: Analysis of individual environmental particles using modern methods of electron microscopy and X-ray microanalysis, J. Electron Spectrosc., 150, 260-274, 10.1016/j.elspec.2005.06.008, 2006.
Laskin, A., Iedema, M. J., and Cowin, J. P.: Time-resolved aerosol collector for CCSEM/EDX single-particle analysis, Aerosol Sci. Tech., 37, 246-260, 10.1080/02786820300945, 2003.
Laskin, A., Moffet, R. C., and Gilles, M. K.: Chemical Imaging of Atmospheric Particles, Accounts Chem. Res., 52, 3419-3431, 10.1021/acs.accounts.9b00396, 2019.
Laskin, A., Gilles, M. K., Knopf, D. A., Wang, B. B., and China, S.: Progress in the Analysis of Complex Atmospheric Particles, Annu. Rev. Anal. Chem., 9, 117-143, 10.1146/annurev-anchem-071015-041521, 2016.
Laskin, A., Moffet, R. C., Gilles, M. K., Fast, J. D., Zaveri, R. A., Wang, B. B., Nigge, P., and Shutthanandan, J.: Tropospheric chemistry of internally mixed sea salt and organic particles: Surprising reactivity of NaCl with weak organic acids, J. Geophys. Res., 117, D15302, 10.1029/2012jd017743, 2012.
Lata, N. N., Zhang, B., Schum, S., Mazzoleni, L., Brimberry, R., Marcus, M. A., Cantrell, W. H., Fialho, P., Mazzoleni, C., and China, S.: Aerosol Composition, Mixing State, and Phase State of Free Tropospheric Particles and Their Role in Ice Cloud Formation, ACS Earth Space Chem., 5, 3499-3510, 10.1021/acsearthspacechem.1c00315, 2021.
Laurila, T. K., Sinclair, V. A., and Gregow, H.: Climatology, variability, and trends in near-surface wind speeds over the North Atlantic and Europe during 1979-2018 based on ERA5, International Journal of Climatology, 41, 2253-2278, 10.1002/joc.6957, 2021.
Lee, H. D., Morris, H. S., Laskina, O., Sultana, C. M., Lee, C., Jayarathne, T., Cox, J. L., Wang, X. F., Hasenecz, E. S., DeMott, P. J., Bertram, T. H., Cappa, C. D., Stone, E. A., Prather, K. A., Grassian, V. H., and Tivanski, A. V.: Organic Enrichment, Physical Phase State, and Surface Tension Depression of Nascent Core-Shell Sea Spray Aerosols during Two Phytoplankton Blooms, ACS Earth Space Chem., 4, 650-660, 10.1021/acsearthspacechem.0c00032, 2020.
Li, J. N. and Knopf, D. A.: Representation of Multiphase OH Oxidation of Amorphous Organic Aerosol for Tropospheric Conditions, Environ. Sci. Technol., 55, 7266-7275, 10.1021/acs.est.0c07668, 2021.
Marcolli, C.: Deposition nucleation viewed as homogeneous or immersion freezing in pores and cavities, Atmos. Chem. Phys., 14, 2071-2104, 10.5194/acp-14-2071-2014, 2014.
Marcolli, C.: Technical note: Fundamental aspects of ice nucleation via pore condensation and freezing including Laplace pressure and growth into macroscopic ice, Atmos. Chem. Phys., 20, 3209-3230, 10.5194/acp-20-3209-2020, 2020.

McCluskey, C. S., Hill, T. C. J., Sultana, C. M., Laskina, O., Trueblood, J., Santander, M. V., Beall, C. M., Michaud, J. M., Kreidenweis, S. M., Prather, K. A., Grassian, V., and DeMott, P. J.: A Mesocosm Double Feature: Insights into the Chemical Makeup of Marine Ice Nucleating Particles, J. Atmos. Sci., 75, 2405-2423, 10.1175/jas-d-17-0155.1, 2018.
McCluskey, C. S., Hill, T. C. J., Malfatti, F., Sultana, C. M., Lee, C., Santander, M. V., Beall, C. M., Moore, K. A., Cornwell, G. C., Collins, D. B., Prather, K. A., Jayarathne, T., Stone, E. A., Azam, F., Kreidenweis, S. M., and DeMott, P. J.: A Dynamic Link between Ice Nucleating Particles Released in Nascent Sea Spray Aerosol and Oceanic Biological Activity during Two Mesocosm Experiments, J. Atmos. Sci., 74, 151-166, 10.1175/jas-d-16-0087.1, 2017.
McCoy, D. T., Field, P., Gordon, H., Elsaesser, G. S., and Grosvenor, D. P.: Untangling causality in midlatitude aerosol-cloud adjustments, Atmos. Chem. Phys., 20, 4085-4103, 10.5194/acp-20-4085-2020, 2020.
McCoy, D. T., Field, P., Frazer, M. E., Zelinka, M. D., Elsaesser, G. S., Mulmenstadt, J., Tan, I., Myers, T. A., and Lebo, Z. J.: Extratropical Shortwave Cloud Feedbacks in the Context of the Global Circulation and Hydrological Cycle, Geophys. Res. Lett., 49, 11, 10.1029/2021gl097154, 2022.
Moffet, R. C., Tivanski, A. V., and Gilles, M. K.: Scanning X-ray Transmission Microscopy: Applications in Atmospheric Aerosol Research, in: Fundamentals and Applications in Aerosol Spectroscopy, edited by: Signorell, R., and Reid, J. P., Taylor and Francis Books, Inc., 419–462, 2010.
Moffet, R. C., Roedel, T. C., Kelly, S. T., Yu, X. Y., Carroll, G. T., Fast, J., Zaveri, R. A., Laskin, A., and Gilles, M. K.: Spectro-microscopic measurements of carbonaceous aerosol aging in Central California, Atmos. Chem. Phys., 13, 10445-10459, 10.5194/acp-13-10445-2013, 2013.
Mülmenstädt, J., Sourdeval, O., Delanoe, J., and Quaas, J.: Frequency of occurrence of rain from liquid-, mixed-, and ice-phase clouds derived from A-Train satellite retrievals, Geophys. Res. Lett., 42, 6502-6509, 10.1002/2015gl064604, 2015.
Mülmenstädt, J., Salzmann, M., Kay, J. E., Zelinka, M. D., Ma, P. L., Nam, C., Kretzschmar, J., Hornig, S., and Quaas, J.: An underestimated negative cloud feedback from cloud lifetime changes, Nature Climate Change, 11, 508-513, 10.1038/s41558-021-01038-1, 2021.
Murray, B. J. and Liu, X.: Ice-nucleating particles and their effects on clouds and radiation, in: Aerosols and Climate, edited by: Carslaw, K. S., Elsevier, Amsterdam, NEtherlands, 619-649, 10.1016/B978-0-12-819766-0.00014-6, 2022.
Murray, B. J., O'Sullivan, D., Atkinson, J. D., and Webb, M. E.: Ice nucleation by particles immersed in supercooled cloud droplets, Chem. Soc. Rev., 41, 6519-6554, 10.1039/c2cs35200a, 2012.
Niemand, M., Möhler, O., Vogel, B., Vogel, H., Hoose, C., Connolly, P., Klein, H., Bingemer, H., DeMott, P., Skrotzki, J., and Leisner, T.: A Particle-Surface-Area-Based Parameterization of Immersion Freezing on Desert Dust Particles, J. Atmos. Sci., 69, 3077-3092, 10.1175/jas-d-11-0249.1, 2012.
O'Dowd, C. D., Facchini, M. C., Cavalli, F., Ceburnis, D., Mircea, M., Decesari, S., Fuzzi, S., Yoon, Y. J., and Putaud, J. P.: Biogenically driven organic contribution to marine aerosol, Nature, 431, 676-680, 10.1038/nature02959, 2004.
Peter, T., Marcolli, C., Spichtinger, P., Corti, T., Baker, M. B., and Koop, T.: When dry air is too humid, Science, 314, 1399-1402, 10.1126/science.1135199, 2006.
Pham, D. Q., O'Brien, R., Fraund, M., Bonanno, D., Laskina, O., Beall, C., Moore, K. A., Forestieri, S., Wang, X., Lee, C., Sultana, C., Grassian, V., Cappa, C. D., Prather, K. A., and Moffet, R. C.: Biological Impacts on Carbon Speciation and Morphology of Sea Spray Aerosol, ACS Earth Space Chem., 10.1021/acsearthspacechem.7b00069, 2017.
Pruppacher, H. R. and Klett, J. D.: Microphysics of Clouds and Precipitation, Kluwer Academic Publishers, Dordrecht1997.
Raveh-Rubin, S.: Dry Intrusions: Lagrangian Climatology and Dynamical Impact on the Planetary Boundary Layer, J. Clim., 30, 6661-6682, 10.1175/jcli-d-16-0782.1, 2017.
Rigg, Y. J., Alpert, P. A., and Knopf, D. A.: Immersion freezing of water and aqueous ammonium sulfate droplets initiated by humic-like substances as a function of water activity, Atmos. Chem. Phys., 13, 6603-6622, 10.5194/acp-13-6603-2013, 2013.
Schnell, R. C.: Ice nuclei produced by laboratory cultured marine phytoplankton, Geophys. Res. Lett., 2, 500-502, 1975.
Schnell, R. C. and Vali, G.: Biogenic Ice Nuclei: Part I. Terrestrial and Marine Sources, J. Atmos. Sci., 33, 1554-1564, 1976.
Shiraiwa, M., Ammann, M., Koop, T., and Poeschl, U.: Gas uptake and chemical aging of semisolid organic aerosol particles, Proc. Natl. Acad. Sci. U. S. A., 108, 11003-11008, 10.1073/pnas.1103045108, 2011.
Stein, A. F., Draxler, R. R., Rolph, G. D., Stunder, B. J. B., Cohen, M. D., and Ngan, F.: NOAA's HYSPLIT atmospheric transport and dispersion modeling system, Bull. Amer. Meteorol. Soc., 96, 2059-2077, 10.1175/bams-d-14-00110.1, 2015.
Storelvmo, T.: Aerosol Effects on Climate via Mixed-Phase and Ice Clouds, in: Annu. Rev. Earth. Planet Sci., Vol 45, edited by: Jeanloz, R., and Freeman, K. H., Annual Review of Earth and Planetary Sciences, 199-222, 10.1146/annurev-earth-060115-012240, 2017.
Stull, R. B.: An Introduction to Boundary Layer Meteorology, Kluwer Academics Publishers, Dordrecht, 667 pp.1988.
Thompson, S. K.: Sample-size for estimating multinomial proportions, Am. Stat., 41, 42-46, 10.2307/2684318, 1987.
Tobo, Y., DeMott, P. J., Hill, T. C. J., Prenni, A. J., Swoboda-Colberg, N. G., Franc, G. D., and Kreidenweis, S. M.: Organic matter matters for ice nuclei of agricultural soil origin, Atmos. Chem. Phys., 14, 8521–8531, 10.5194/acp-14-8521-2014, 2014.
Tomlin, J. M., Jankowski, K. A., Veghte, D. P., China, S., Wang, P. W., Fraund, M., Weis, J., Zheng, G. J., Wang, Y., Rivera-Adorno, F., Raveh-Rubin, S., Knopf, D. A., Wang, J., Gilles, M. K., Moffet, R. C., and Laskin, A.: Impact of dry intrusion events on the composition

and mixing state of particles during the winter Aerosol and Cloud Experiment in the Eastern North Atlantic (ACE-ENA), Atmos. Chem. Phys., 21, 18123-18146, 10.5194/acp-21-18123-2021, 2021.
Vali, G.: Quantitative evaluation of experimental results on heterogeneous freezing nucleation of supercooled liquids, J. Atmos. Sci., 28, 402-409, 1971.
Vali, G., DeMott, P. J., Möhler, O., and Whale, T. F.: Technical Note: A proposal for ice nucleation terminology, Atmos. Chem. Phys., 15, 10263-10270, 10.5194/acp-15-10263-2015, 2015.
Wang, B. and Knopf, D. A.: Heterogeneous ice nucleation on particles composed of humic-like substances impacted by O3, J. Geophys. Res., 116, D03205, 10.1029/2010jd014964, 2011.
Wang, B., Lambe, A. T., Massoli, P., Onasch, T. B., Davidovits, P., Worsnop, D. R., and Knopf, D. A.: The deposition ice nucleation and immersion freezing potential of amorphous secondary organic aerosol: Pathways for ice and mixed-phase cloud formation, J. Geophys. Res., 117, D16209, 10.1029/2012jd018063, 2012a.
Wang, B., Laskin, A., Roedel, T., Gilles, M. K., Moffet, R. C., Tivanski, A. V., and Knopf, D. A.: Heterogeneous ice nucleation and water uptake by field-collected atmospheric particles below 273 K, J. Geophys. Res., 117, D00V19, 10.1029/2012JD017446, 2012b.
Wang, J., Wood, R., Jensen, M. P., Chiu, J. C., Liu, Y. G., Lamer, K., Desai, N., Giangrande, S. E., Knopf, D. A., Kollias, P., Laskin, A., Liu, X. H., Lu, C. S., Mechem, D., Mei, F., Starzec, M., Tomlinson, J., Wang, Y., Yum, S. S., Zheng, G. J., Aiken, A. C., Azevedo, E. B., Blanchard, Y., China, S., Dong, X. Q., Gallo, F., Gao, S. N., Ghate, V. P., Glienke, S., Goldberger, L., Hardin, J. C., Kuang, C. A., Luke, E. P., Matthews, A. A., Miller, M. A., Moffet, R., Pekour, M., Schmid, B., Sedlacek, A. J., Shaw, R. A., Shilling, J. E., Sullivan, A., Suski, K., Veghte, D. P., Weber, R., Wyant, M., Yeom, J., Zawadowicz, M., and Zhang, Z. B.: Aerosol and Cloud Experiments in the Eastern North Atlantic (ACE-ENA), Bull. Amer. Meteorol. Soc., 103, E619-E641, 10.1175/bams-d-19-0220.1, 2022.
Wang, Y., Zheng, X. J., Dong, X. Q., Xi, B. K., Wu, P., Logan, T., and Yung, Y. L.: Impacts of long-range transport of aerosols on marine-boundary-layer clouds in the eastern North Atlantic, Atmos. Chem. Phys., 20, 14741-14755, 10.5194/acp-20-14741-2020, 2020.
Wang, Y., Zheng, G. J., Jensen, M. P., Knopf, D. A., Laskin, A., Matthews, A. A., Mechem, D., Mei, F., Moffet, R., Sedlacek, A. J., Shilling, J. E., Springston, S., Sullivan, A., Tomlinson, J., Veghte, D., Weber, R., Wood, R., Zawadowicz, M. A., and Wang, J.: Vertical profiles of trace gas and aerosol properties over the eastern North Atlantic: variations with season and synoptic condition, Atmos. Chem. Phys., 21, 11079-11098, 10.5194/acp-21-11079-2021, 2021.
Welti, A., Thomson, E. S., Schrod, J., Ickes, L., David, R. O., Dong, Z., and Kanji, Z. A.: Overview of ambient ice nucleation measurements from 1949 – 2000, EGU General Assembly 2023, Vienna, Austria, 10.5194/egusphere-egu23-1458, 2023, 2023.
Wilbourn, E. K., Thornton, D. C. O., Ott, C., Graff, J., Quinn, P. K., Bates, T. S., Betha, R., Russell, L. M., Behrenfeld, M. J., and Brooks, S. D.: Ice Nucleation by Marine Aerosols Over the North Atlantic Ocean in Late Spring, J. Geophys. Res.-Atmos., 125, 17, 10.1029/2019jd030913, 2020.
Wilson, T. W., Ladino, L. A., Alpert, P. A., Breckels, M. N., Brooks, I. M., Browse, J., Burrows, S. M., Carslaw, K. S., Huffman, J. A., Judd, C., Kilthau, W. P., Mason, R. H., McFiggans, G., Miller, L. A., Najera, J. J., Polishchuk, E., Rae, S., Schiller, C. L., Si, M., Temprado, J. V., Whale, T. F., Wong, J. P. S., Wurl, O., Yakobi-Hancock, J. D., Abbatt, J. P. D., Aller, J. Y., Bertram, A. K., Knopf, D. A., and Murray, B. J.: A marine biogenic source of atmospheric ice-nucleating particles, Nature, 525, 234-238, 10.1038/nature14986, 2015.
Wolf, M. J., Zhang, Y., Zawadowicz, M. A., Goodell, M., Froyd, K., Freney, E., Sellegri, K., Rosch, M., Cui, T. Q., Winter, M., Lacher, L., Axisa, D., DeMott, P. J., Levin, E. J. T., Gute, E., Abbatt, J., Koss, A., Kroll, J. H., Surratt, J. D., and Cziczo, D. J.: A biogenic secondary organic aerosol source of cirrus ice nucleating particles, Nat. Commun., 11, 4834, 10.1038/s41467-020-18424-6, 2020.
Wood, R., Wyant, M., ., Bretherton, C. S., Remillard, J., Kollias, P., Fletcher, J., Stemmler, J., de Szoeke, S., Yuter, S., Miller, M., Mechem, D., Tselioudis, G., Chiu, J. C., Mann, J. A. L., O'Connor, E. J., Hogan, R. J., Dong, X. Q., Miller, M., Ghate, V., Jefferson, A., Min, Q. L., Minnis, P., Palikonda, R., Albrecht, B., Luke, E., Hannay, C., and Lin, Y. L.: Clouds, aerosols, and precipitation in the marine boundary layer An ARM Mobile Facility Deployment, Bull. Amer. Meteorol. Soc., 96, 419-439, 10.1175/bams-d-13-00180.1, 2015.
Zawadowicz, M. A., Suski, K., Liu, J. M., Pekour, M., Fast, J., Mei, F., Sedlacek, A. J., Springston, S., Wang, Y., Zaveri, R. A., Wood, R., Wang, J., and Shilling, J. E.: Aircraft measurements of aerosol and trace gas chemistry in the eastern North Atlantic, Atmos. Chem. Phys., 21, 7983-8002, 10.5194/acp-21-7983-2021, 2021.
Zheng, G. J., Sedlacek, A. J., Aiken, A. C., Feng, Y., Watson, T. B., Raveh-Rubin, S., Uin, J., Lewis, E. R., and Wang, J.: Long-range transported North American wildfire aerosols observed in marine boundary layer of eastern North Atlantic, Environ. Int., 139, 16, 10.1016/j.envint.2020.105680, 2020.
Zheng, G. J., Wang, Y., Aiken, A. C., Gallo, F., Jensen, M. P., Kollias, P., Kuang, C. G., Luke, E., Springston, S., Uin, J., Wood, R., and Wang, J.: Marine boundary layer aerosol in the eastern North Atlantic: seasonal variations and key controlling processes, Atmospheric Chemistry and Physics, 18, 17615-17635, 10.5194/acp-18-17615-2018, 2018.
Zobrist, B., Marcolli, C., Pedernera, D. A., and Koop, T.: Do atmospheric aerosols form glasses?, Atmos. Chem. Phys., 8, 5221-5244, 2008.
Zobrist, B., Koop, T., Luo, B. P., Marcolli, C., and Peter, T.: Heterogeneous ice nucleation rate coefficient of water droplets coated by a nonadecanol monolayer, J. Phys. Chem. C, 111, 2149-2155, 10.1021/Jp066080w, 2007.

**Table 1: Information about collection of particle samples including sample name, substrate type, sampling altitude (above mean sea level), estimated marine boundary layer height, date and time period, and presence of a dry intrusion event.**

| | Sample Pair # | Sampling Altitude (a.m.s.l.) / m | Boundary Layer Height (a.m.s.l.) / m | Sampling Date | Sampling Time | Dry Intrusion |
|---|---|---|---|---|---|---|
| S-MBL1 | $Si_3N_4$ | Min: 33<br>Max: 67 | 1600 | 07 Jul 2017 | 1:25:32 PM - 1:35:33 PM | |
| | TEM | Min: 53<br>Max: 583 | | | 1:35:33 PM - 1:45:35 PM | |
| W-MBL1-DI | $Si_3N_4$ | Min: 26<br>Max: 277 | 1400 | 25 Jan 2018 | 2:20:59 PM - 2:28:01 PM | yes |
| | TEM 1 | Min: 34<br>Max: 1891 | | | 2:13:56 PM - 2:20:59 PM | |
| | TEM 2 | Min: 215<br>Max: 272 | | | 2:28:01 PM - 2:35:03 PM | |
| W-MBL2-DI | $Si_3N_4$ | Min: 27<br>Max: 73 | 700 | 01 Feb 2018 | 11:22:10 AM - 11:29:13 AM | yes |
| | TEM | Min: 28<br>Max: 62 | | | 1:29:02 PM - 1:36:04 PM | |
| S-FT1 | $Si_3N_4$ | Min: 1283<br>Max: 1839 | ~1000 | 15 Jul 2017 | 1:31:22 PM - 1:41:24 PM | |
| | TEM | Min: 663<br>Max: 1283 | | | 1:41:24 PM - 1:51:26 PM | |
| W-FT1-DI | $Si_3N_4$ | Min:1436<br>Max: 1710 | 1400 | 25 Jan 2018 | 1:45:45 PM - 1:52:48 PM | yes |
| | TEM 1 | Min: 1436 | | | 1:38:43 PM - 1:45:45 PM | |

| | | | | | | |
|---|---|---|---|---|---|---|
| | TEM 2 | Max: 1455<br>Min: 1587<br>Max: 1679 | | | 1:52:48 PM - 1:59:51PM | |
| W-FT2 | $Si_3N_4$ | Min: 73<br>Max: 1513 | 1100 | 30 Jan 2018 | 1:28:24 PM - 1:35:27 PM | |
| | TEM | Min: 1503<br>Max: 1512 | | | 1:21:21 PM - 1:28:24 PM | |
| W-FT3-DI | $Si_3N_4$ | Min: 4021<br>Max: 4101 | ~1000 - 3500 | 19 Feb 2018 | 1:40:35 PM - 1:47:38 PM | yes |
| | TEM | Min: 4028<br>Max: 4076 | | | 1:33:32 PM - 1:40:35 PM | |

835

**Table 2: Summary of particle sample information: Sample name, number of particles examined by scanning transmission X-ray microscopy with near-edge X-ray absorption fine structure spectroscopy (STXM/NEXAFS) and computer-controlled scanning electron microscopy (CCSEM) and CCSEM sample surface area examined. CCSEM determined average area equivalent diameter, number of particles examined for ice formation, and estimated particle surface area involved in ice formation experiments. Optical microscopy (OMI) estimated particle surface area involved in ice formation experiments.**

| Sample ID | Number of particles examined by STXM | Number of particles examined by CCSEM | CCSEM Area examined / $mm^2$ | CCSEM Average area equivalent diameter / µm | CCSEM Number of particles examined for ice formation / $mm^2$ | CCSEM Particle surface area estimate for ice formation / $cm^2$ | OMI Particle surface area estimate for ice formation / $cm^2$ |
|---|---|---|---|---|---|---|---|
| S-MBL1 | 352 | 1660 | 0.022 | 0.32±0.18 | 56845±1421 | $(1.21\pm0.03)\times10^{-4}$ | $6\times10^{-4}$ |
| W-MBL1-DI | 241 | - | - | - | - | - | $8.6\times10^{-5}$ |
| W-MBL2-DI | 196 | 966 | 0.080 | 0.22±0.13 | 9160±229 | $(9.50\pm0.2)\times10^{-6}$ | $6.5\times10^{-5}$ |
| S-FT1 | 371 | 3633 | 0.022 | 0.22±0.16 | 124409±3110 | $(1.45\pm0.04)\times10^{-4}$ | $1\times10^{-4}$ |
| W-FT1-DI | 121 | 3994 | 0.080 | 0.23±0.16 | 37875±947 | $(4.79\pm0.1)\times10^{-5}$ | $4\times10^{-4}$ |
| W-FT2 | 71 | 953 | 0.080 | 0.15±0.09 | 9037±275 | $(4.39\pm0.1)\times10^{-6}$ | $1\times10^{-5}$ |
| W-FT3-DI | 151 | 3160 | 0.218 | 0.19±0.13 | 10992±275 | $(9.47\pm0.2)\times10^{-6}$ | $2.5\times10^{-5}$ |

**Table 3. Information about identified ice-nucleating particles (INPs) including temperature and humidity conditions, scanning electron microscopy (SEM) derived area equivalent diameter, and particle-type classification.**

| INP ID | Ice nucleation temperature / K | Ice nucleation humidity $RH_{ice}$ / % | Area equivalent diameter / µm | Classification |
|---|---|---|---|---|
| S-FT1 | 243 | 135.1 | 1.89 | Dust |
| S-FT1 | 233 | 130.3 | 3.93 | Sea Salt |
| S-FT1 | 233 | 130.3 | 1.98 | Sea Salt |
| S-FT1 | 223 | 120.4 | 0.65 | Sea Salt |
| S-FT1 | 223 | 120.4 | 0.49 | Other |
| S-FT1 | 223 | 120.4 | 0.55 | Sea Salt |
| S-FT1 | 223 | 120.4 | 0.73 | Sea Salt + Sulfate |
| W-FT1-DI | 223 | 134.4 | 0.92 | Sea Salt + Sulfate |
| W-FT1-DI | 223 | 134..4 | 0.69 | Sea Salt + Sulfate |
| W-FT1-DI | 223 | 114.3 | 1.02 | Sea Salt + Sulfate |
| W-FT3-DI | 223 | 133.0 | 10.45 | Carbonaceous |
| W-FT3-DI | 223 | 133.0 | 11.02 | Carbonaceous |

**Table 4. Parameters for derivation of the immersion freezing (IMF) and deposition ice nucleation (DIN) heterogeneous ice nucleation rate coefficient coefficients ($J_{het}$) and ice nucleation active sites (INAS) density ($n_s$) for marine boundary layer (MBL) and free troposphere (FT) particle samples are given as a function of the water activity criterion, $\Delta a_w$, according to $\log J_{het} = c + m \cdot \Delta a_w$ and $\log n_s = c + m \cdot \Delta a_w$. LCL and UCL represent lower and upper confidence levels at 95%, respectively, for the fit parameters. RMSE indicates root mean square error of the fit.**

| Parameterization | $c$ | $LCL_c$ | $UCL_c$ | $m$ | $LCL_m$ | $UCL_m$ | RMSE |
|---|---|---|---|---|---|---|---|
| MBL IMF $J_{het}$ | 1.128 | -0.2636 | 2.52 | 5.791 | 0.5344 | 11.05 | 0.5988 |
| MBL IMF $n_s$ | 2.207 | 0.8156 | 3.599 | 5.791 | 0.5344 | 11.05 | 0.5988 |
| MBL DIN $J_{het}$ | 2.096 | 1.715 | 2.477 | 3.154 | 1.328 | 4.98 | 0.4731 |
| MBL DIN $n_s$ | 3.175 | 2.795 | 3.556 | 3.154 | 1.328 | 4.98 | 0.4731 |
| FT DIN $J_{het}$ | 1.05 | 0.2942 | 1.805 | 12.18 | 7.15 | 17.21 | 0.5706 |
| FT DIN $n_s$ | 2.129 | 1.373 | 2.884 | 12.18 | 7.15 | 17.21 | 0.5706 |

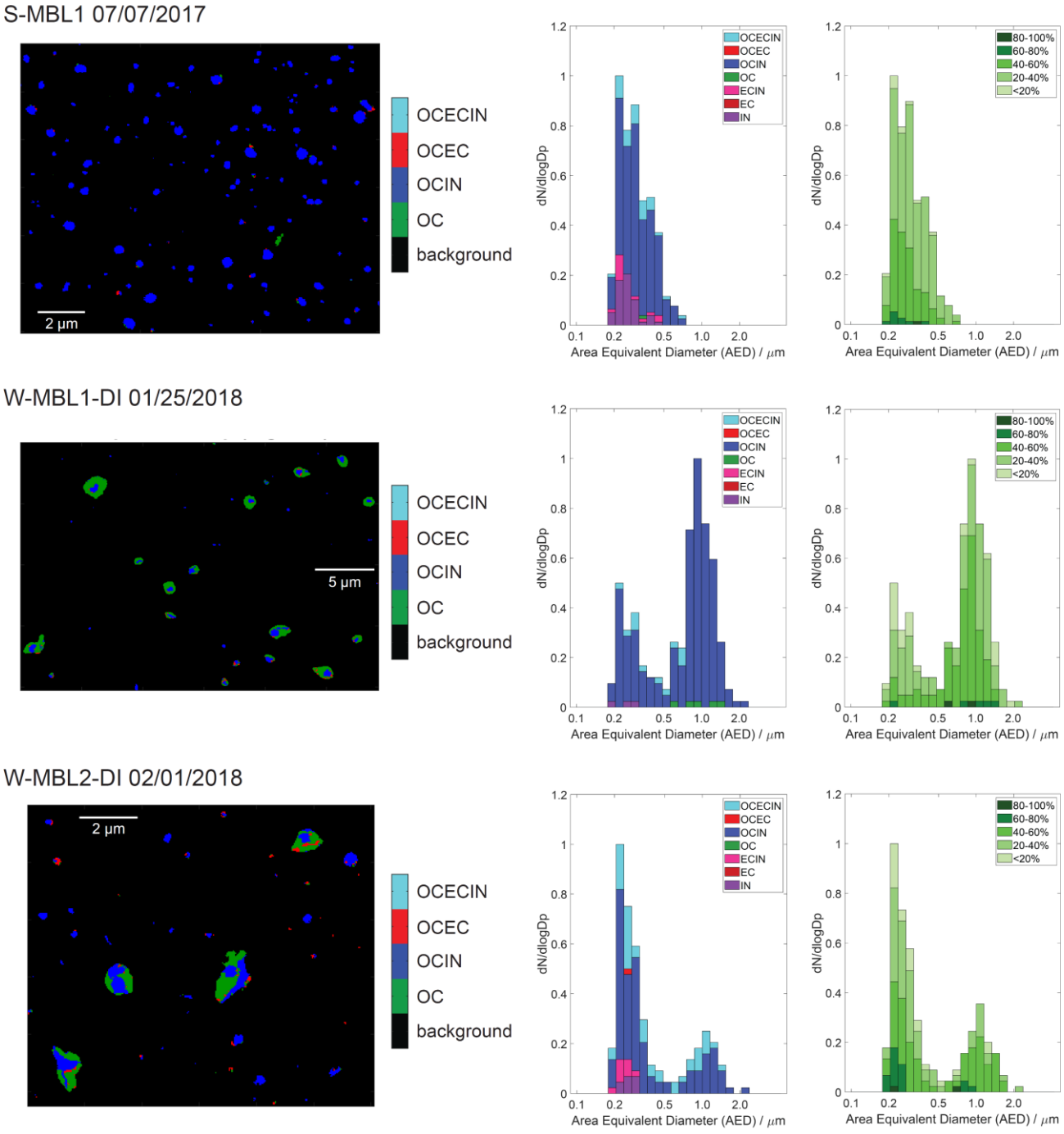


**Figure 1: Representative STXM/NEXAFS analyses of marine boundary layer (MBL) particle samples as indicated by legends. From left to right: false-color particle maps that show particle mixing state composition where OCIN - organic carbonaceous-inorganic, OCEC - organic carbonaceous-elemental carbon, OC - organic carbonaceous. Normalized size-resolved mixing state analysis where IN - inorganic, EC - elemental carbon, OC - organic carbonaceous. Normalized size-resolved organic volume fraction (OVF) per particle where color green intensity represents OC fraction.**

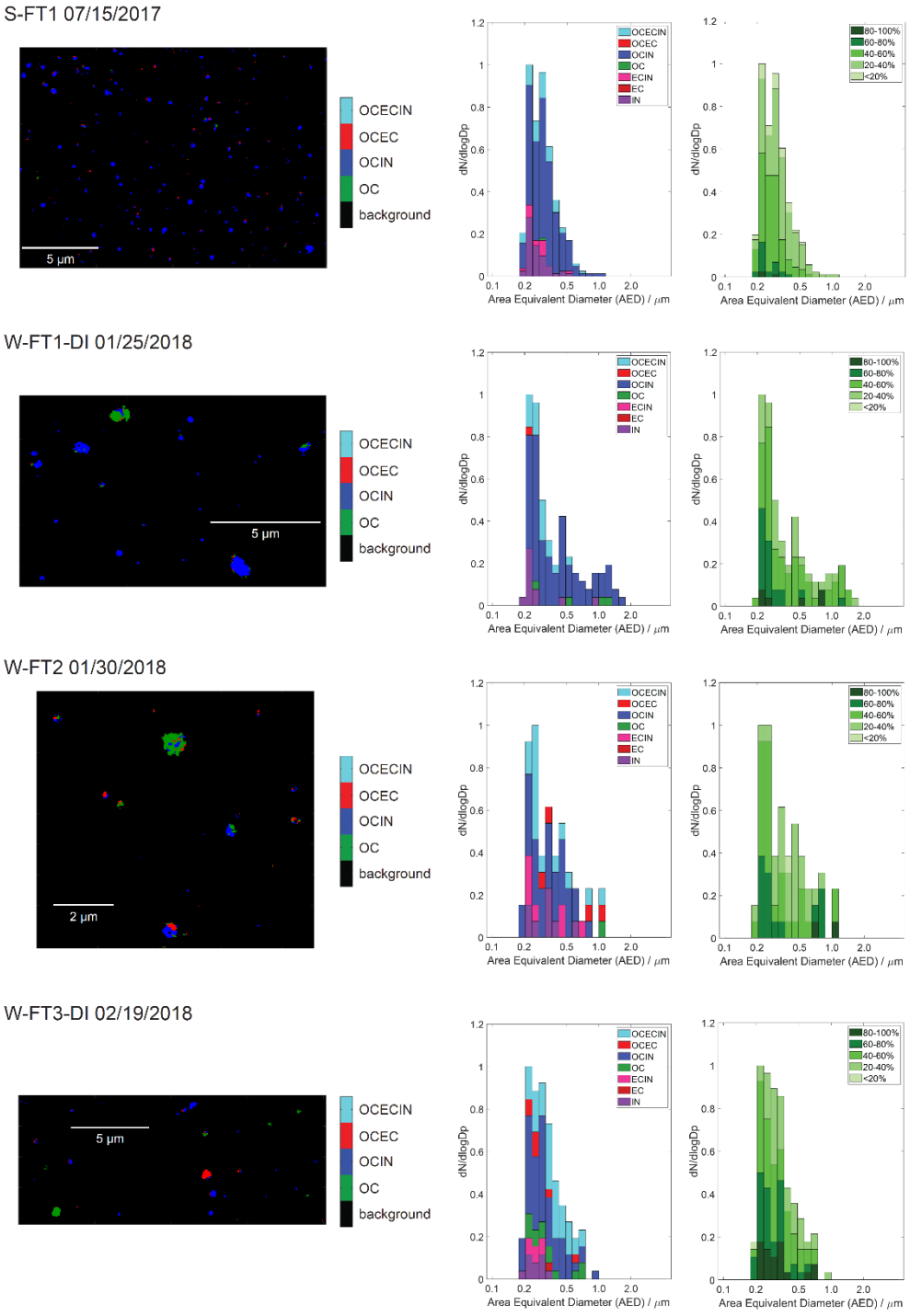


**Figure 2: Representative STXM/NEXAFS analyses of free troposphere (FT) particle samples as indicated. Panels follow description of Fig. 1.**

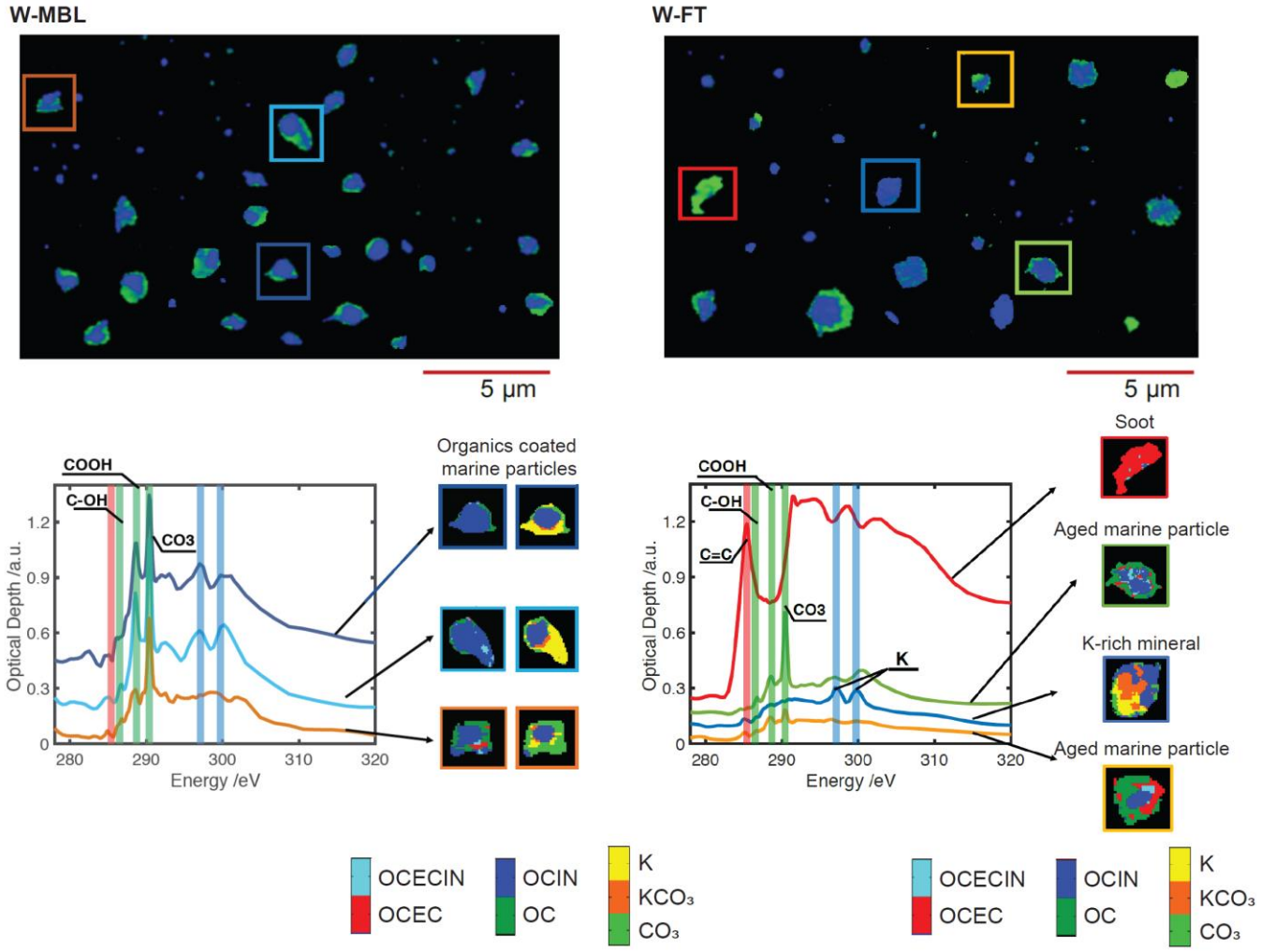


**Figure 3: Representative STXM/NEXAFS analyses of IOP2-MBL and IOP2-FT samples. Upper panels show false-color particle maps where organic dominated particles are in green (organic mass is > 80%) and inorganic dominated particles are blue (inorganic mass is > 80%). Lower panels show high resolution NEXAFS spectra with indicated organic functional groups including C-C double bonds (C=C), alcohol (C-OH), hydroxyl (COOH), carbonate ($CO_3$), and inorganic species potassium (K). Corresponding detailed images of particles and their mixing state are given by legend below where IN - inorganic, EC - elemental carbon, OC - organic carbon, and $KCO_3$ – potassium carbonate.**

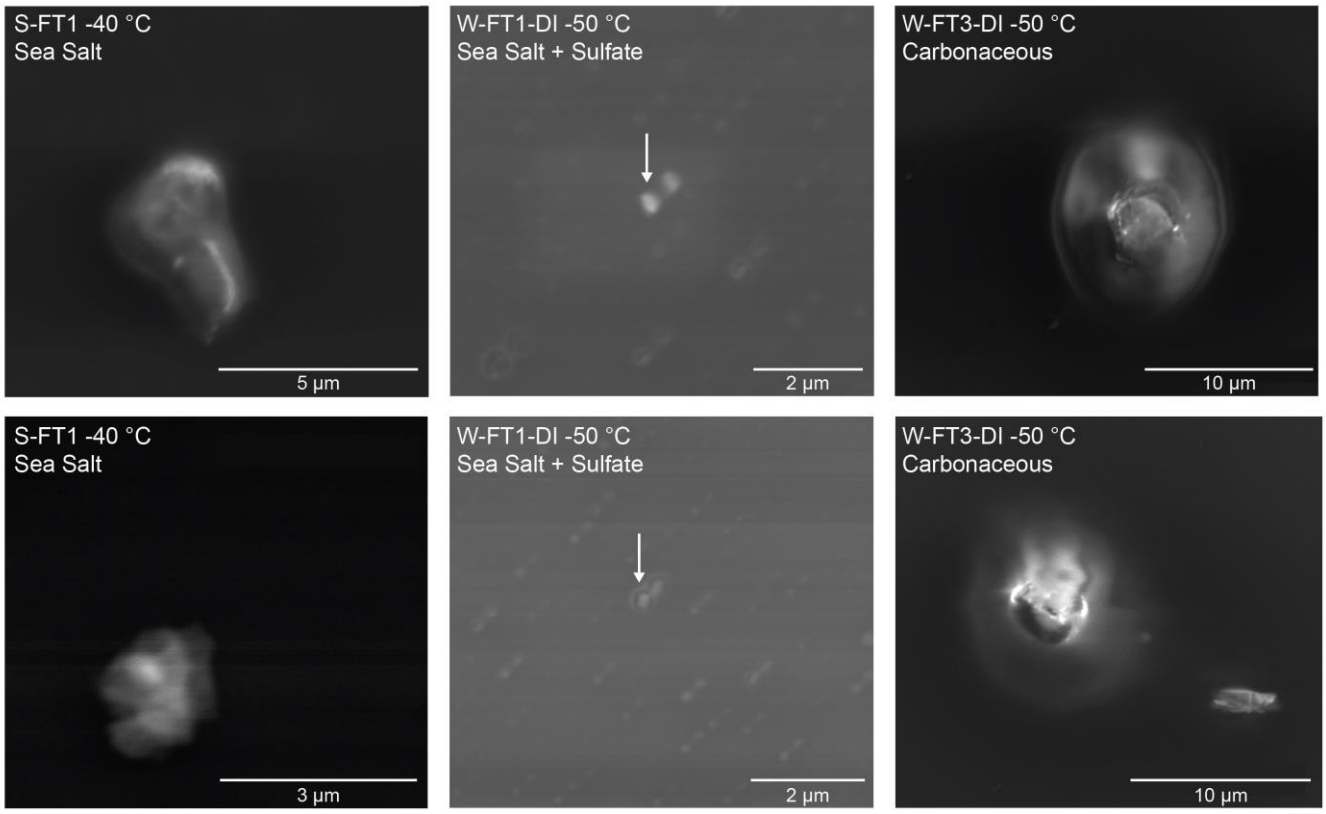


**Figure 4: Identified ice-nucleating particles (INPs) with ice formation temperature indicated. White arrow highlights the INP. ~~The assigned particle types are, starting clockwise from upper left panel: sea salt, sea salt + sulfate, OC, OC, sea salt + sulfate, and sea salt.~~**

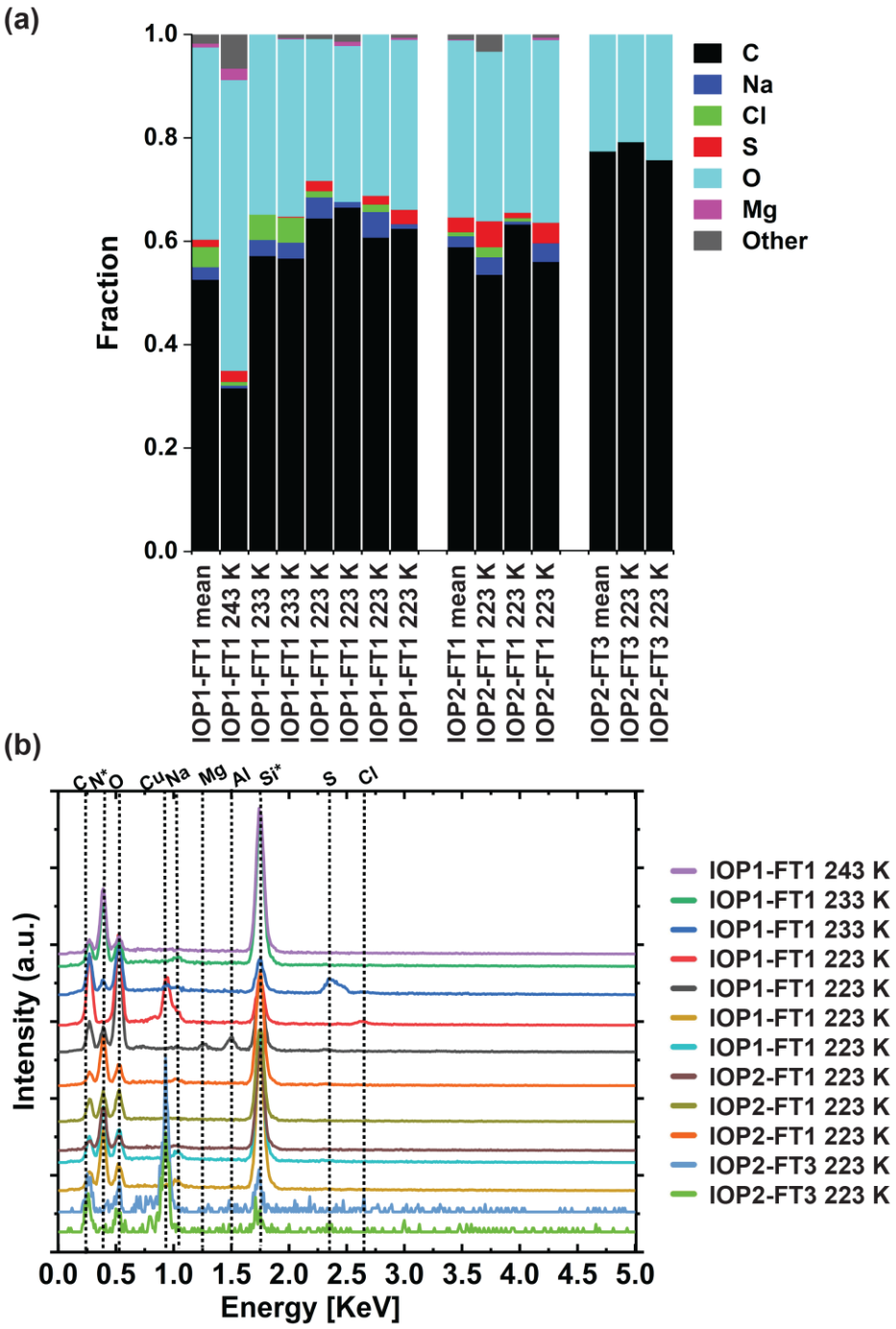


**Figure 5: Composition of experimentally identified INPs. (a) Cumulative atomic percent of elements for 12 identified individual INPs is shown as bars for examined ACE-ENA particle samples. The first column represents the average cumulative atomic percent of elements of the INPs for the specific particle sample. Panel (b) shows representative EDX spectra of identified INPs. * corresponds to the signal from the substrate ($Si_3N_4$-coated silicon wafer chips).**

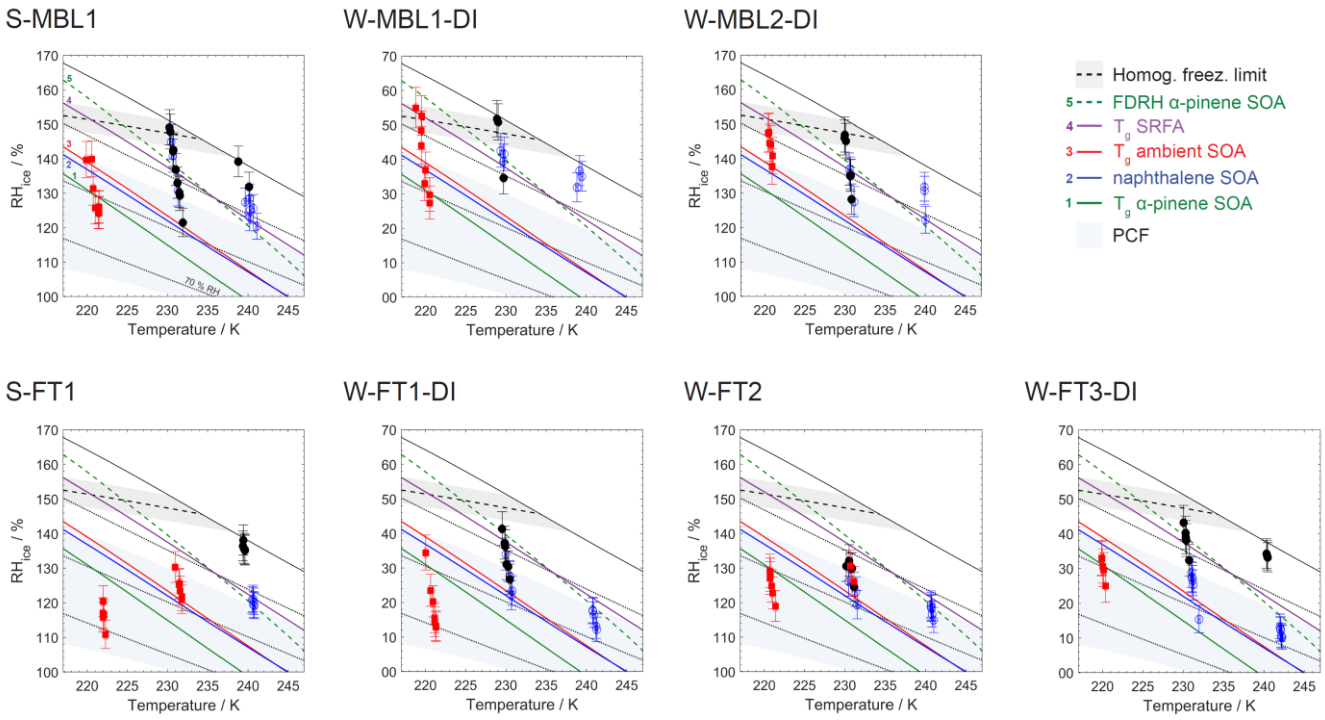


940 **Figure 6: Ice nucleation and water uptake conditions observed for indicated ACE-ENA particle samples are given as a function of *T* and $RH_{ice}$. IMF - Immersion freezing (black solid circles), DIN - deposition ice nucleation (red solid squares), water uptake (blue open circles). The data points and error bars reflect the uncertainties in *T* and $RH_{ice}$. Solid line represents conditions of water saturation (100% RH). Dotted lines indicate constant relative humidity (RH). Dashed line and grey shading represent the homogeneous freezing limit for droplets of 10 µm in size and corresponding uncertainty (Koop, 2004; Koop et al., 2000). The glass**
945 **transition temperature of laboratory generated α-pinene SOA (green line or 1, (Charnawskas et al., 2017)), naphthalene SOA (blue line or 2, (Charnawskas et al., 2017)) field-derived SOA (red line or 3, (Wang et al., 2012a)), and Suwannee River Fulvic Acid particles (dark violet line or 4, (Wang et al., 2012a)) are plotted. The dashed green line (or 5) displays the full deliquescence relative humidity for α-pinene SOA particles, 500 nm in diameter, under the humidification rate of this experiment (Charnawskas et al., 2017). The light bluish area indicates the conditions for pore condensation freezing (PCF) for pore sizes of 7.5 to 20 nm (Marcolli,**
950 **2020, 2014).**

955

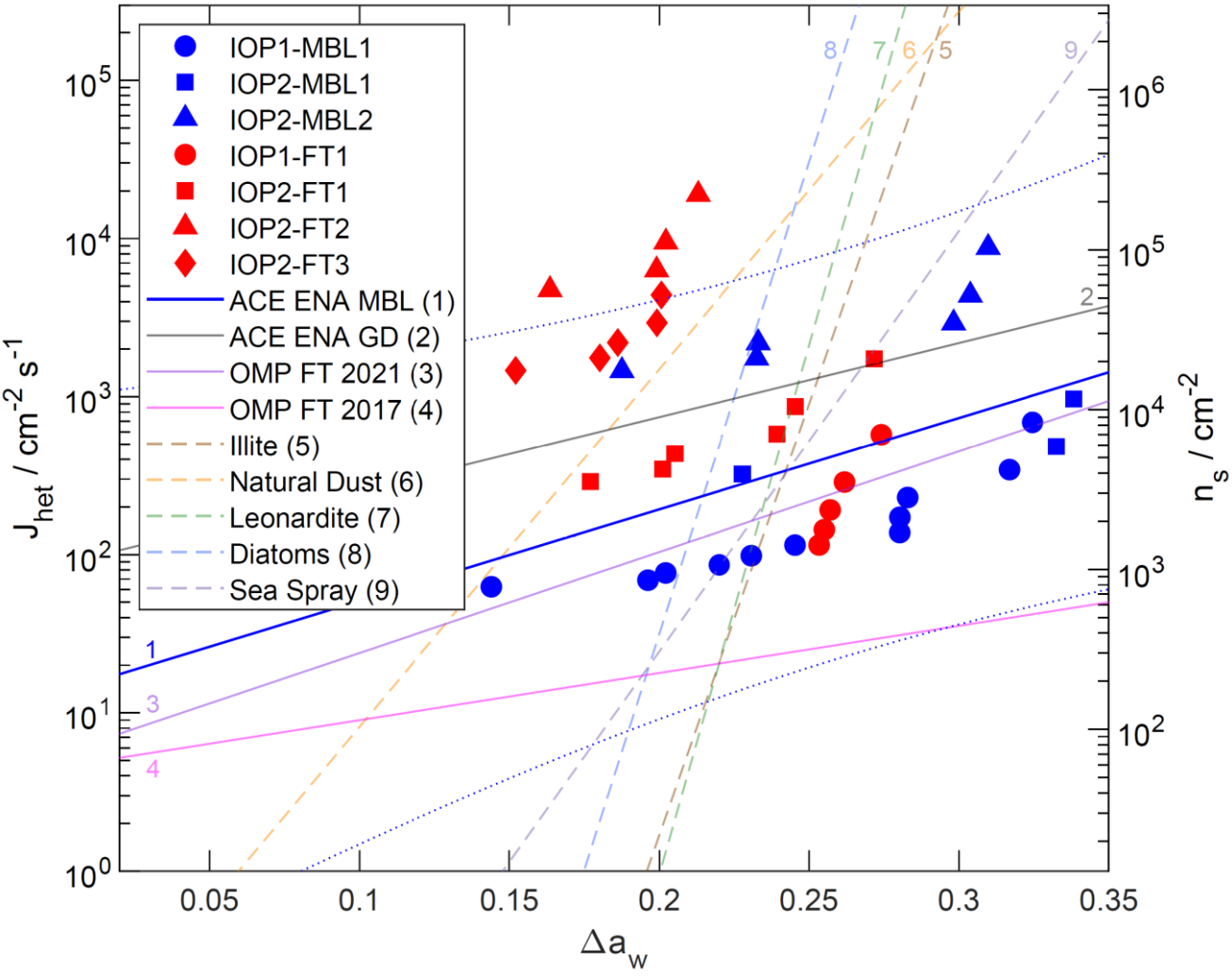


**Figure 7: Immersion freezing (IMF) data of examined ACE-ENA particle samples (solid symbols) and of previous studies (colored lines) as given in legend. Heterogeneous ice nucleation rate coefficients ($J_{het}$) and ice nucleation active sites (INAS) density ($n_s$) are presented as a function of the water activity criterion $\Delta a_w$. Corresponding error bars are given in Fig. S11. Blue solid line represents a linear regression to the newly derived MBL IMF data. Solid black, magenta, and purple lines represent $J_{het}$ and $n_s$ IMF derived from accompanying ACE-ENA ground site INP measurements (ACE-ENA GD), from the Observatory of Mountain Pico (OMP) measurements under free tropospheric (FT) conditions in the Azores on a neighboring island (PMO FT 2017, 2021; (China et al., 2017; Lata et al., 2021)). Please note that only $J_{het}$ was reported for OMP FT 2021 (Lata et al., 2021). Water activity-based IMF $J_{het}$ and $n_s$ for other INP types are given as dashed colored lines as indicated in legend.**

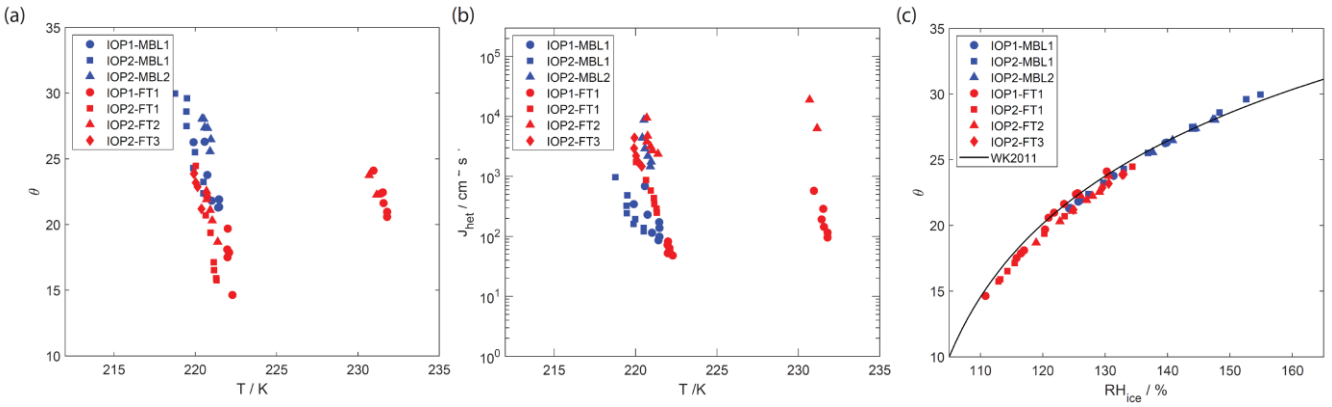


**Figure 8: Deposition ice nucleation (DIN) data of examined ACE-ENA MBL and FT particle samples in blue and red colors, respectively. (a) Heterogeneous ice nucleation rate coefficients ($J_{het}$) as a function of temperature. (b) Contact angles ($\theta$) corresponding to $J_{het}$ values shown in (a). (c) $\theta$ values for relative humidity with respect to ice ($RH_{ice}$) under which DIN was observed. Solid line represents the DIN parameterization by Wang and Knopf (2011). Corresponding error bars are given in Fig. S12.**

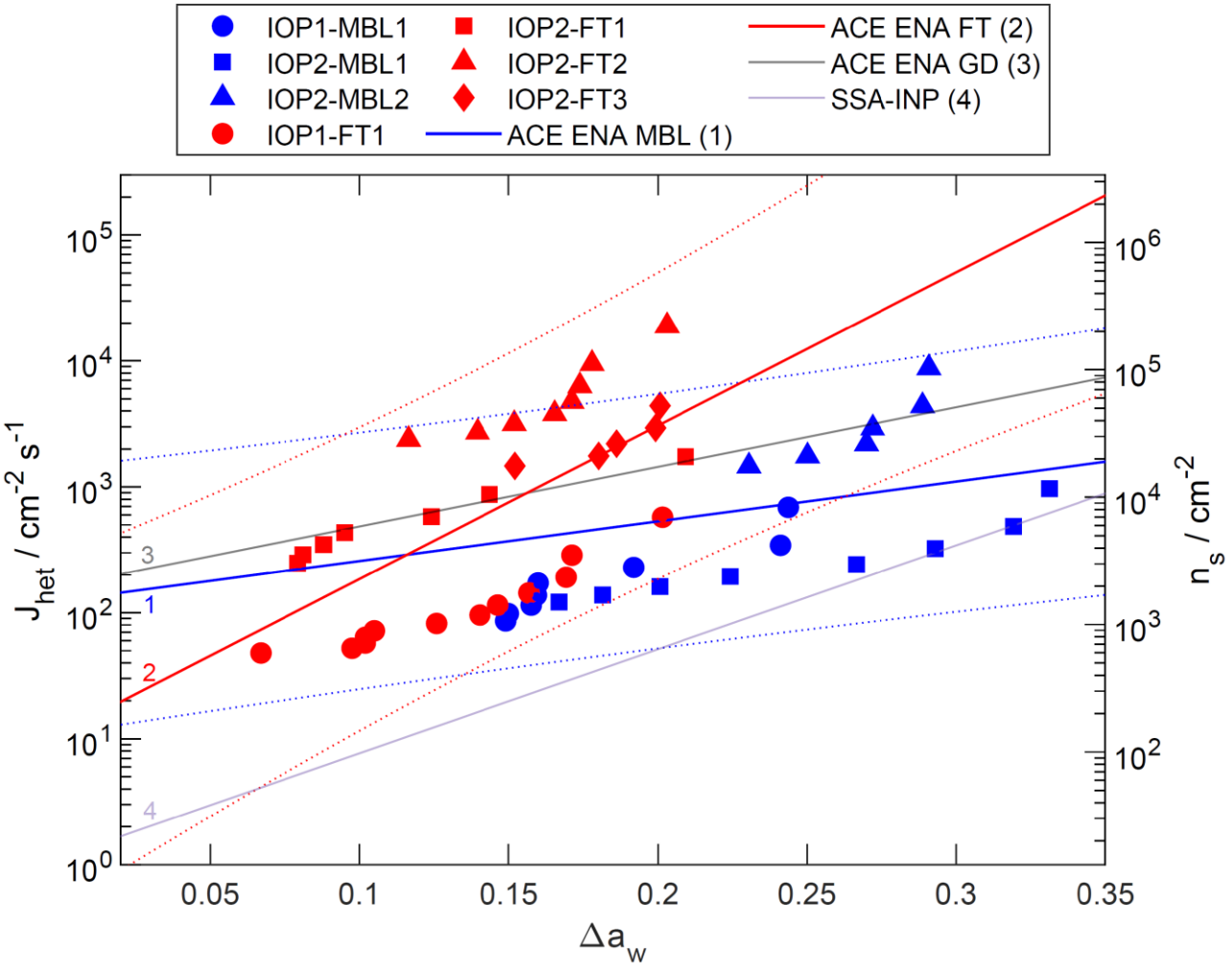


**Figure 9: Deposition ice nucleation (DIN) data of examined ACE-ENA MBL and FT particle samples (blue and red symbols, respectively). Heterogeneous ice nucleation rate coefficients ($J_{het}$) and ice nucleation active sites (INAS) density ($n_s$) are presented. Corresponding error bars are given in Fig. S13. Blue and red solid and dotted black lines represent linear regression fits and associated fit uncertainties for MBL and FT particle samples, respectively. Black line represents the DIN ABIFM parameterization derived from ground site ACE-ENA INP measurements. Purple line represents the water-activity based DIN sea spray aerosol parameterization from Alpert et al. (2022).**

# Supplement of
# Physicochemical characterization of free troposphere and marine boundary layer ice-nucleating particles collected by aircraft in the eastern North Atlantic

Daniel A. Knopf[1,2], Peiwen Wang[1], Benny Wong[1,2], Jay M. Tomlin[3], Daniel P. Veghte[4†], Nurun N. Lata[4], Swarup China[4], Alexander Laskin[3], Ryan C. Moffet[5], Josephine Y. Aller[1], Matthew A. Marcus[6], Jian Wang[7]

[1]School of Marine and Atmospheric Sciences, Stony Brook University, Stony Brook, NY 11794, USA
[2]Department of Chemistry, Stony Brook University, Stony Brook, NY 11794, USA
[3]Department of Chemistry, Purdue University, West Lafayette, IN 47907, USA
[4]Environmental Molecular Sciences Laboratory/Pacific Northwest National Laboratory, Richland, WA 99354, USA
[5]Sonoma Technology, Inc., Petaluma, CA 94954, USA
[6]Advanced Light Source, Lawrence Berkeley National Laboratory, Berkeley, CA 94720, USA
[7]Center for Aerosol Science and Engineering, Department of Energy, Environmental and Chemical Engineering, Washington University in St. Louis, St. Louis, MO 63130, USA

†Current address: Center for Electron Microscopy and Analysis, The Ohio State University, Columbus, OH 43212, USA

*Correspondence to*: Daniel A. Knopf (daniel.knopf@stonybrook.edu)

This Supplement comprises of thirteen figures (S1-S13).

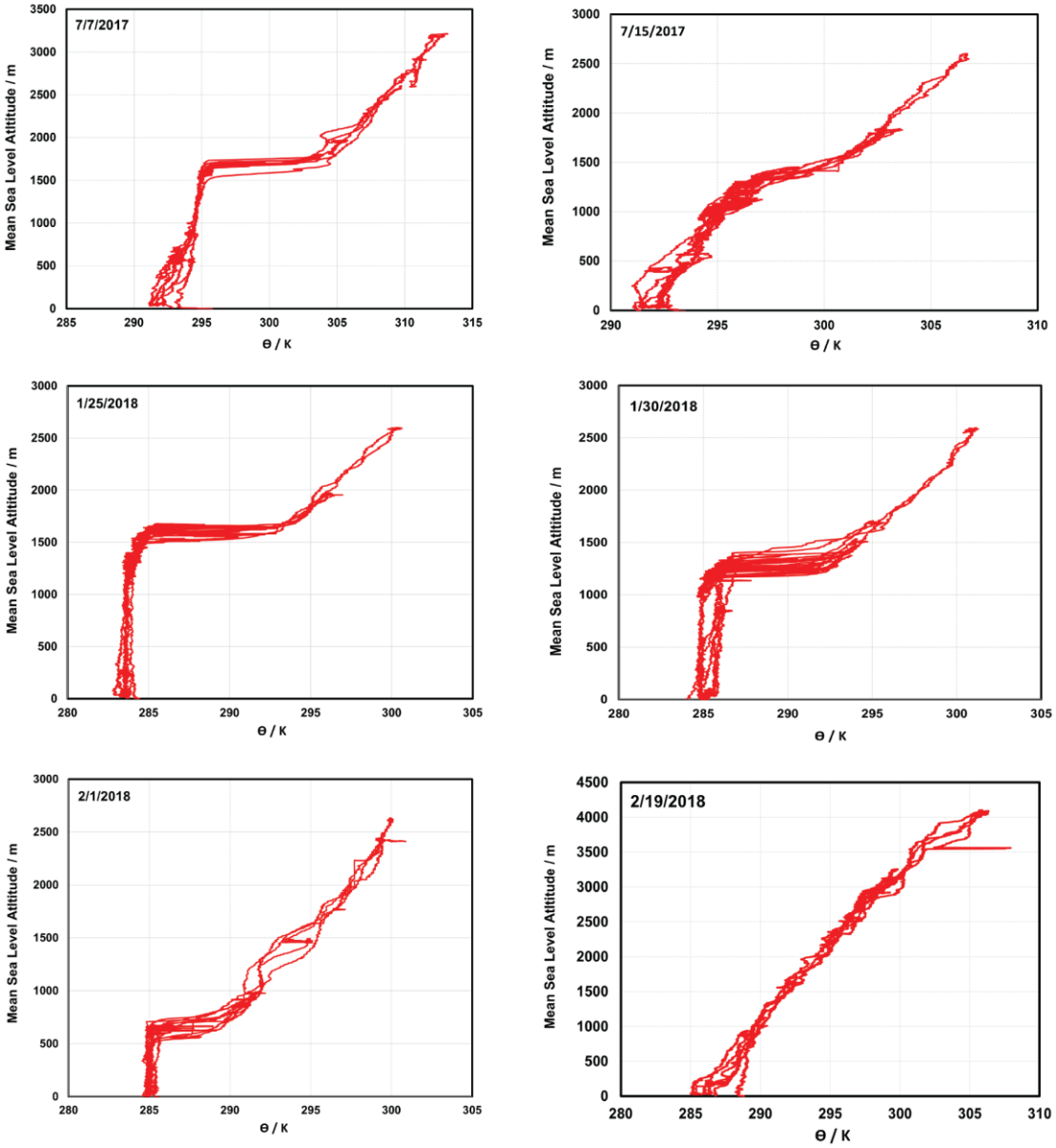


**Figure S1: Flight altitude versus potential temperature (Θ) for each flight date as given in Table 1.**

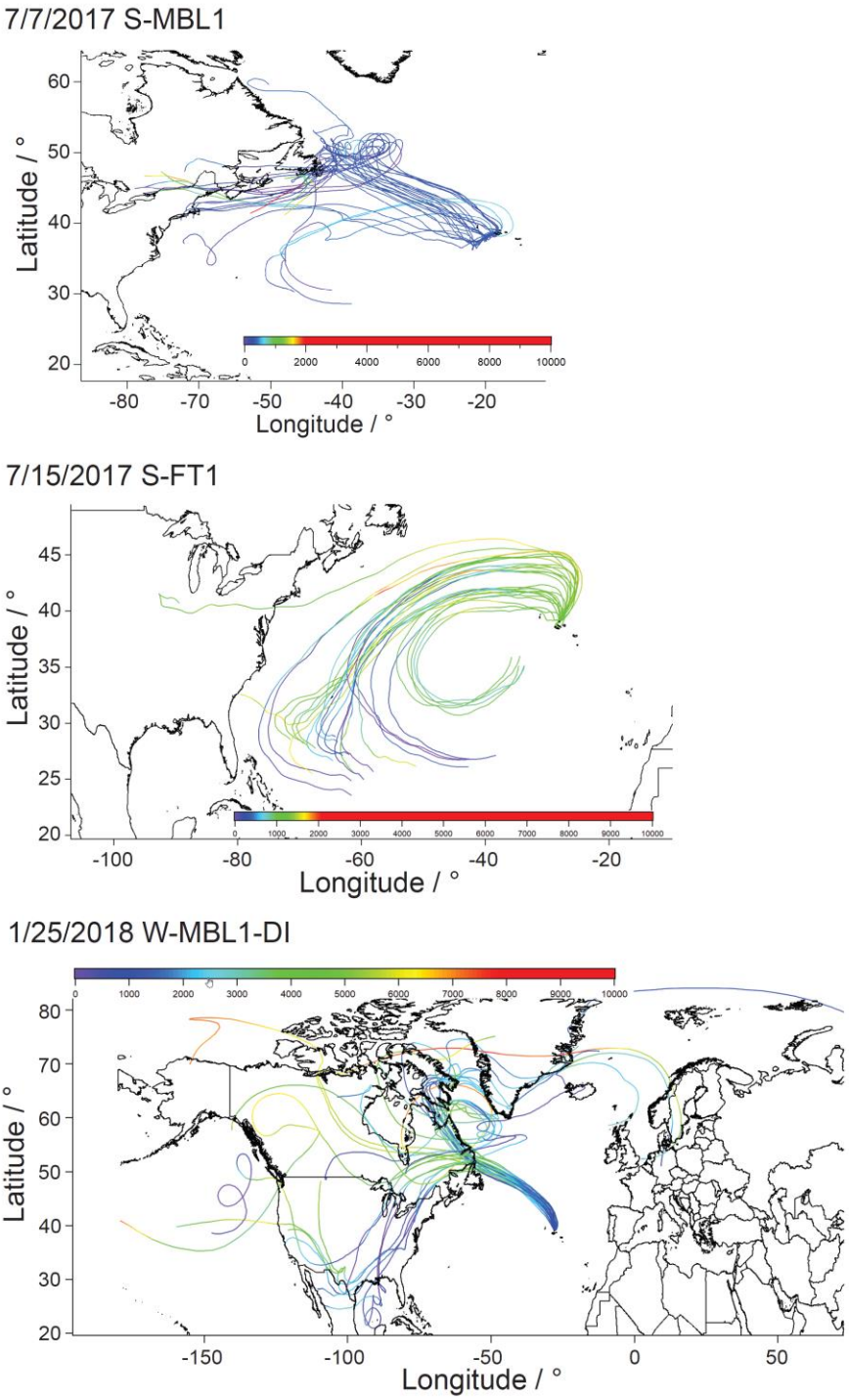


**Figure S2: Representative 10-day backward trajectories for examined airborne-collected marine boundary layer (MBL) and free troposphere (FT) particle samples starting at given sampling altitude. The trajectories are colored by their altitude (m).**

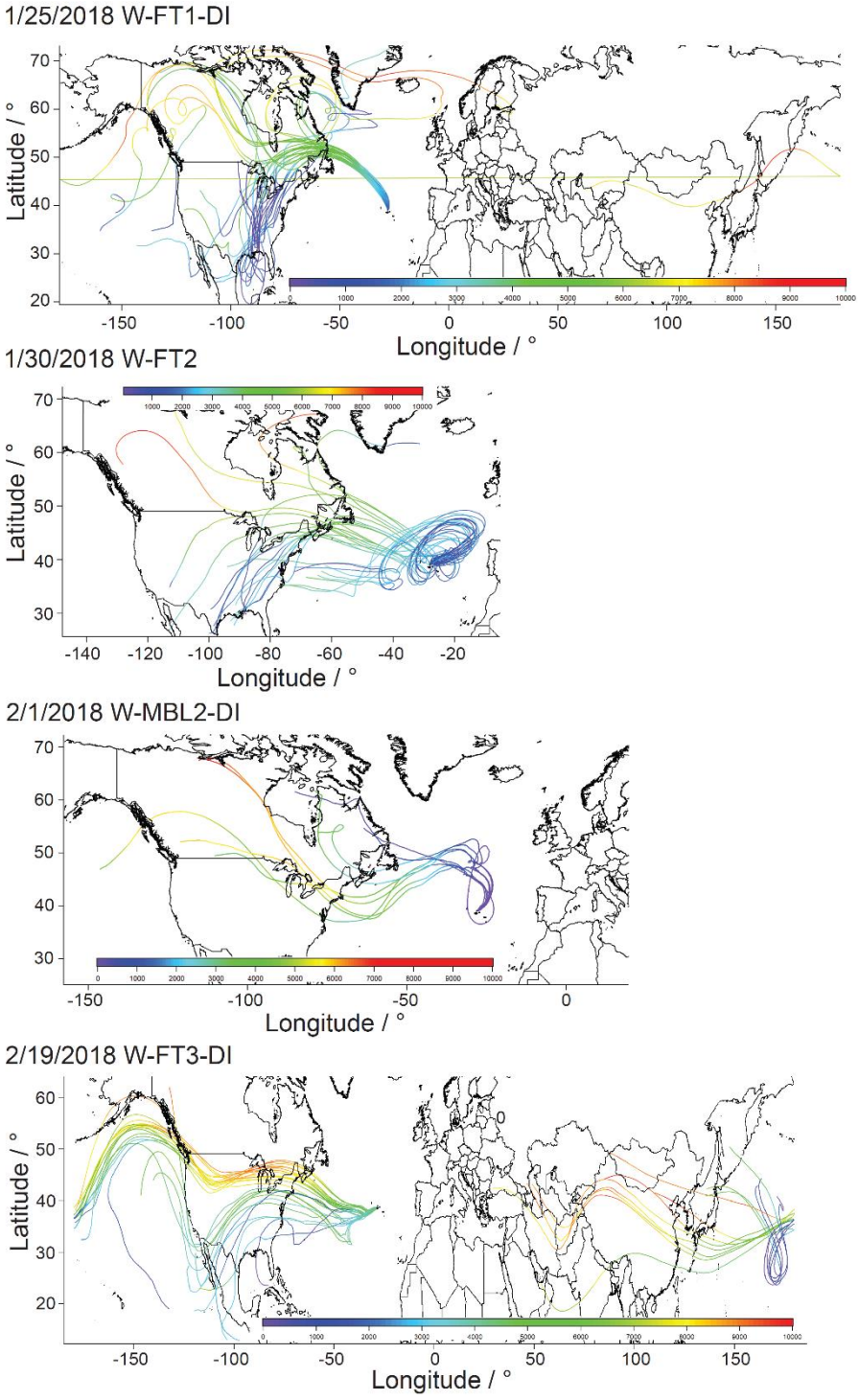


**Figure S3: Representative 10-day backward trajectories for examined airborne-collected marine boundary layer (MBL) and free troposphere (FT) particles starting at given sampling altitude. The trajectories are colored by their altitude (m).**

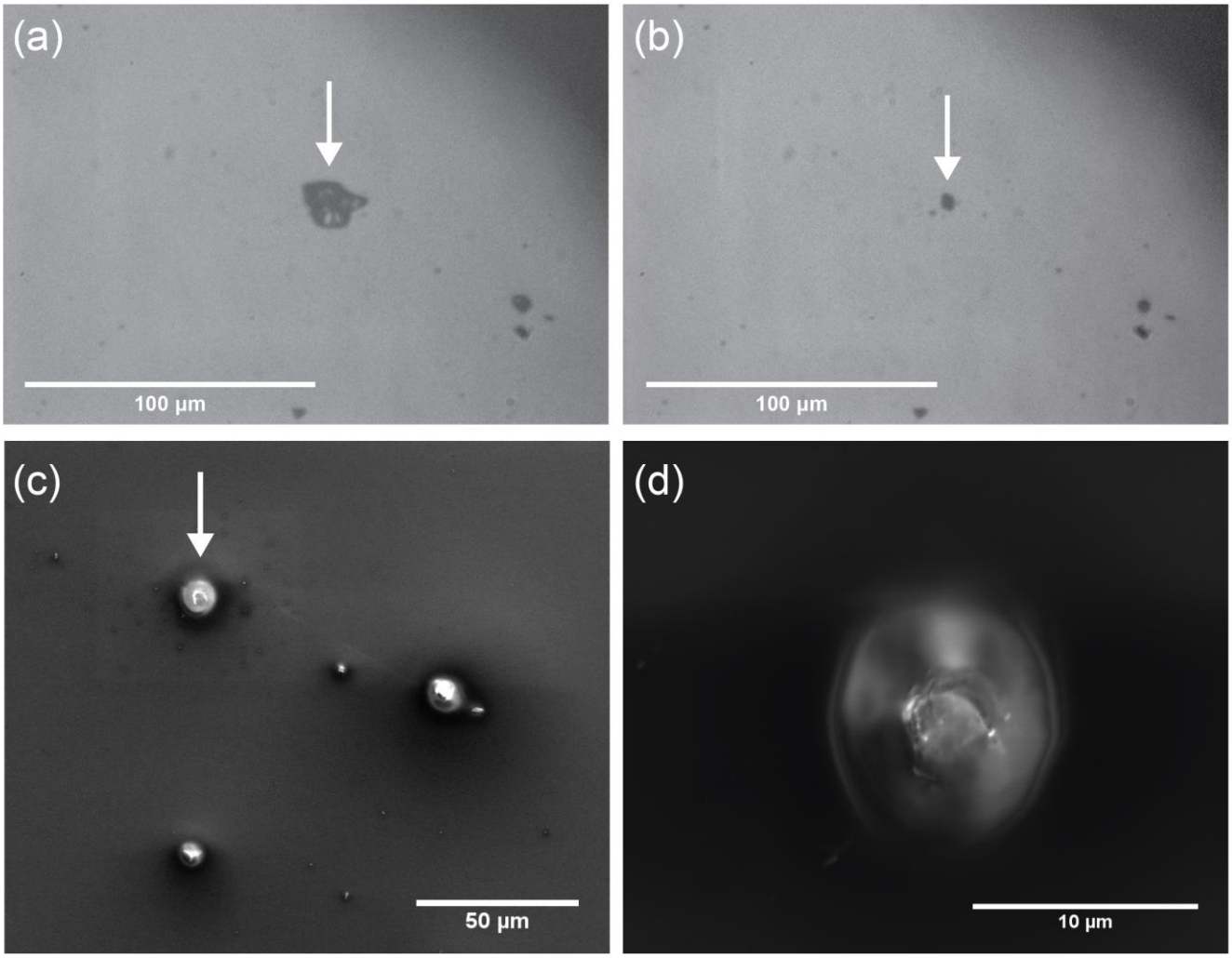


**Figure S4: Procedure to identify the ice nucleating particle (INP) from optical microscope images (panels a and b) in scanning electron microscopy (panels c and d). Panel (b) shows the residual particles after ice crystal sublimation. White arrow indicates the INP.**

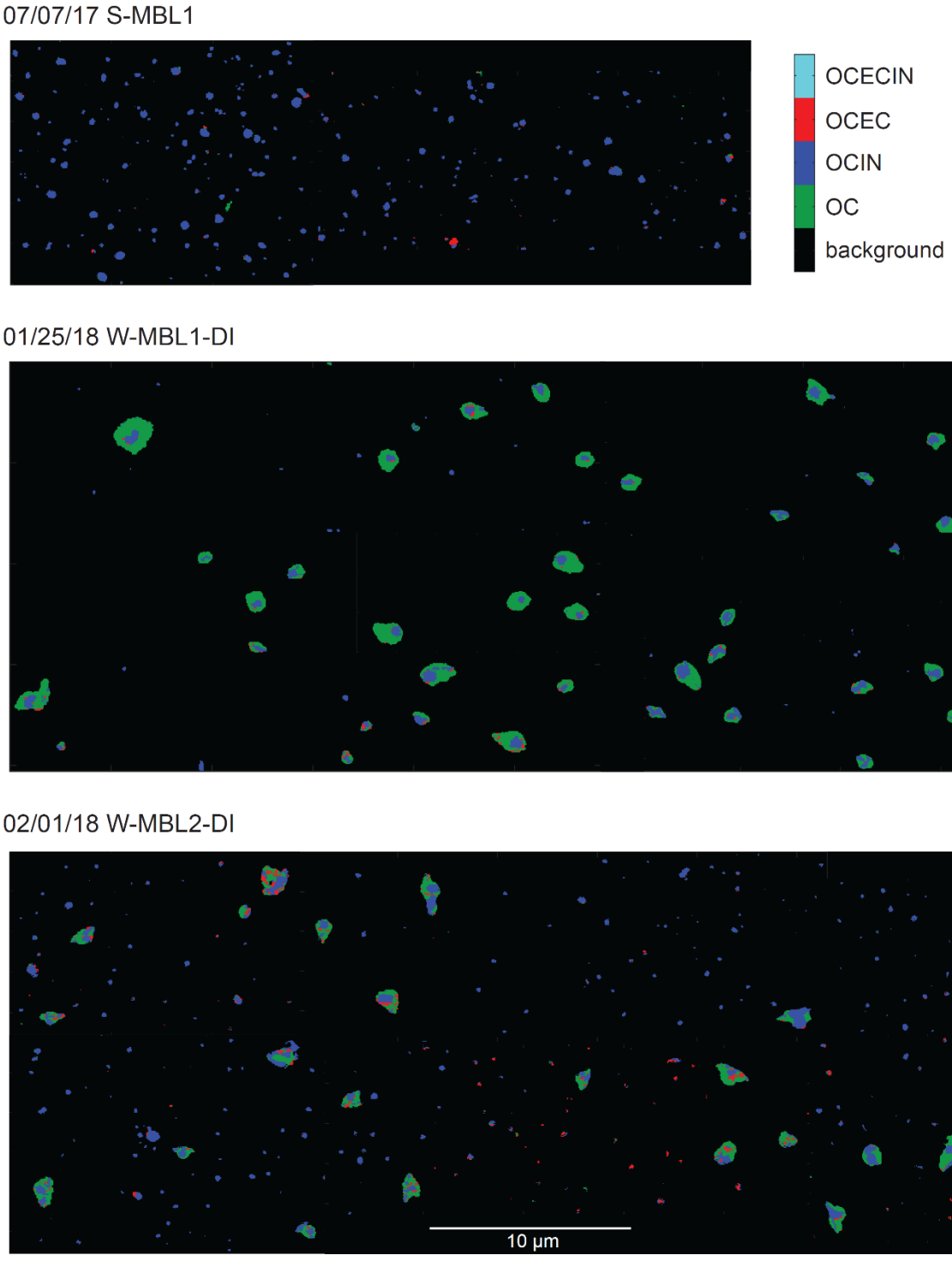


**Figure S5: Representative particle mixing state analysis of particle samples collected in the marine boundary layer (MBL) where IN - inorganic, EC - elemental carbon, and OC - organic carbon. The scale bar holds for all panels.**

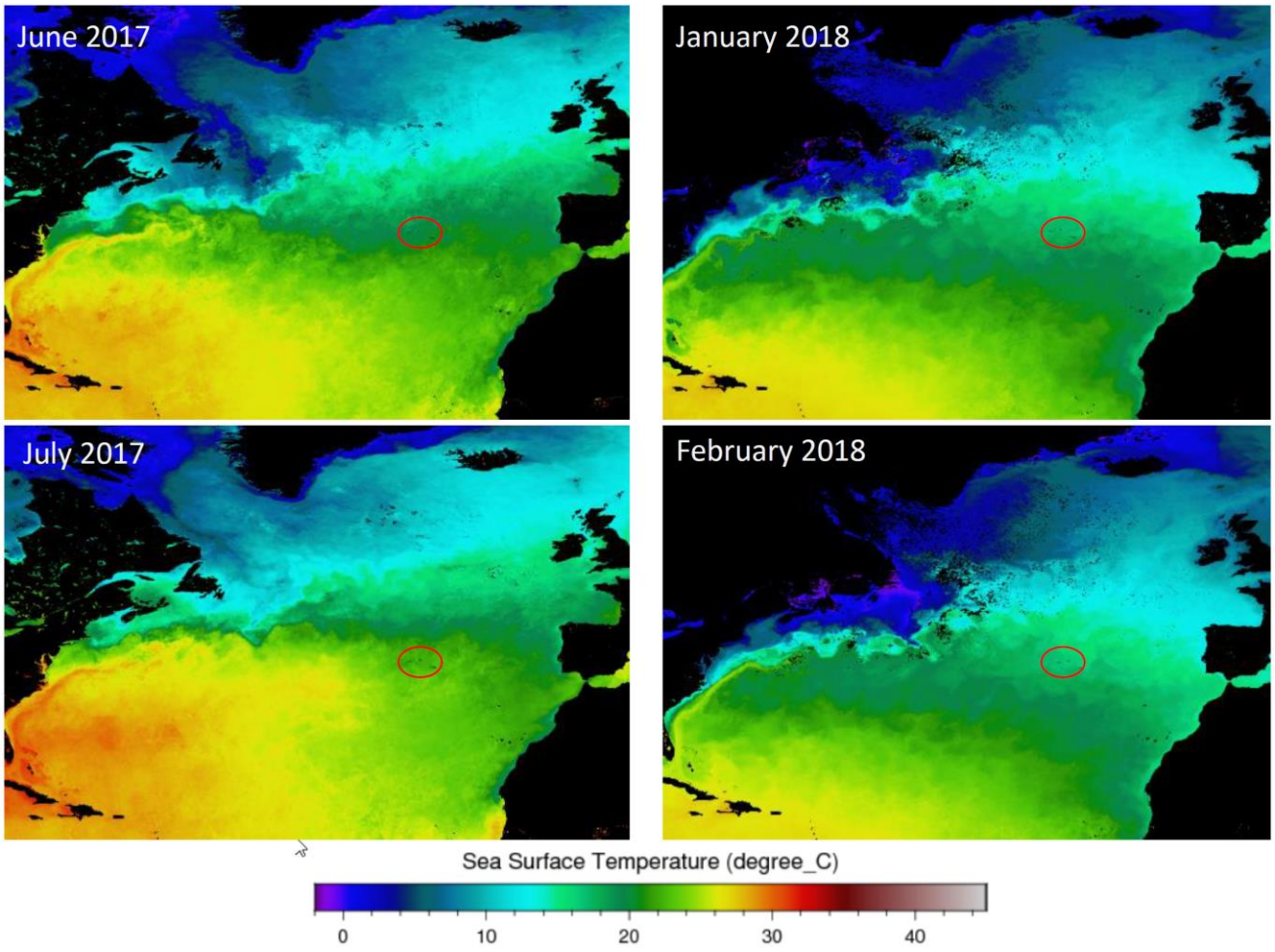


**Figure S6: Monthly mean sea surface temperature derived by Aqua MODIS (Moderate Resolution Imaging Spectroradiometer) during daytime at 11 µm and 4 km resolution (NASA Goddard Space Flight Center, 2019). Red circles indicate location of Azores Islands.**

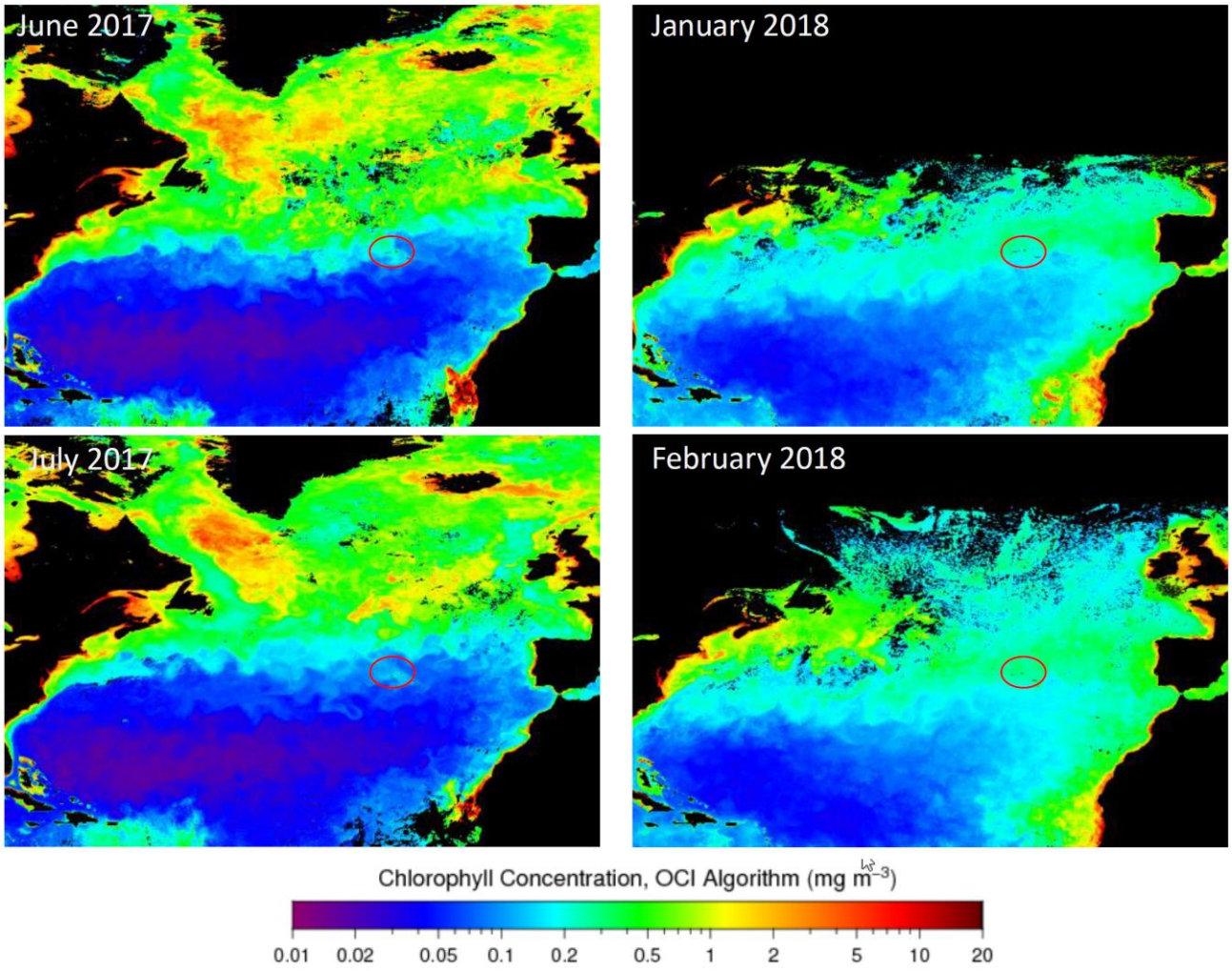


**Figure S7: Monthly mean chlorophyll a concentration derived by Aqua MODIS (Moderate Resolution Imaging Spectroradiometer) at 4 km resolution (NASA Goddard Space Flight Center, 2022). Red circles indicate location of Azores Islands.**

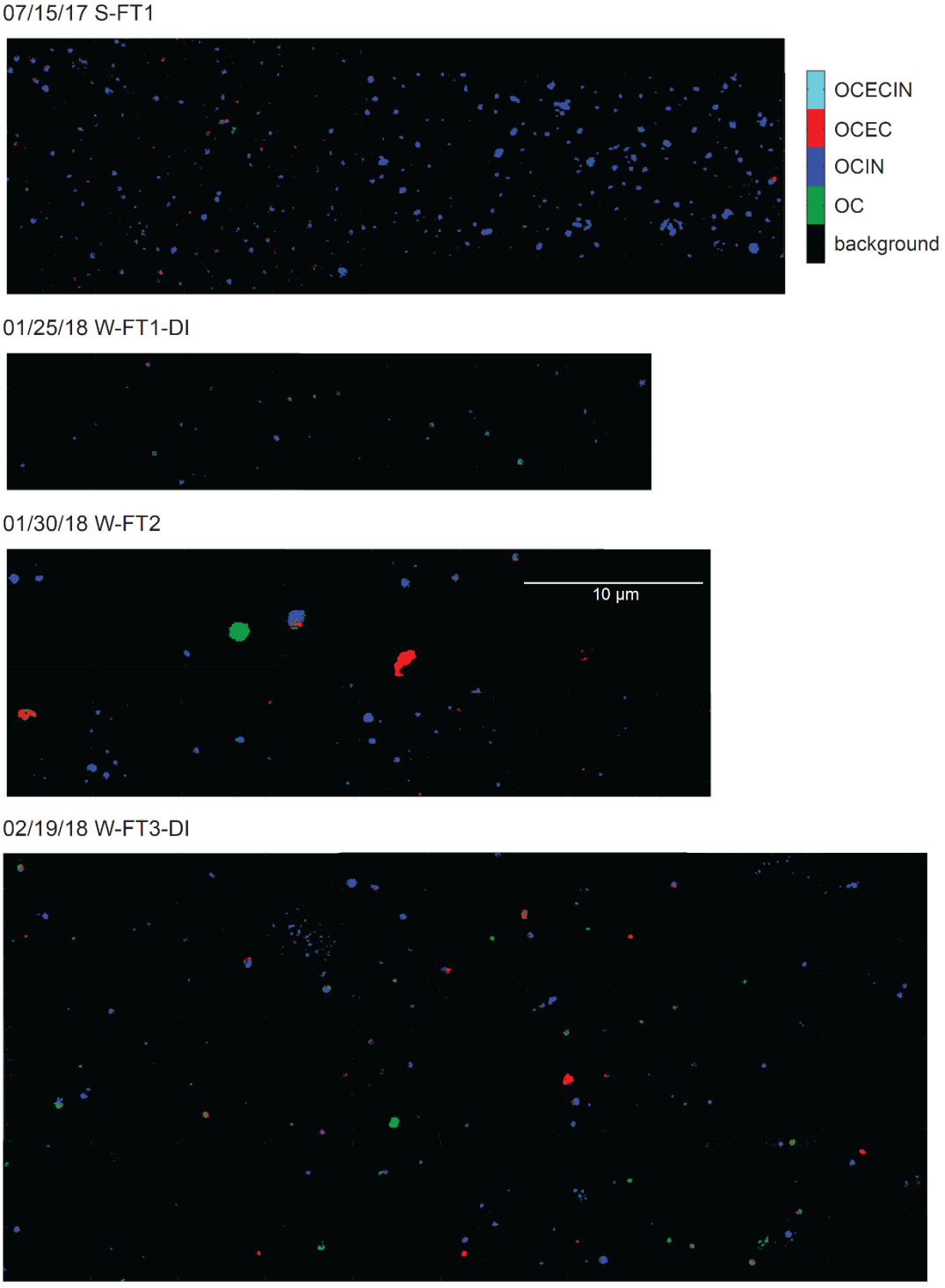


**Figure S8: Representative particle mixing state analysis of particle samples collected in the free troposphere (FT) where IN - inorganic, EC - elemental carbon, and OC - organic carbon. The scale bar holds for all panels.**

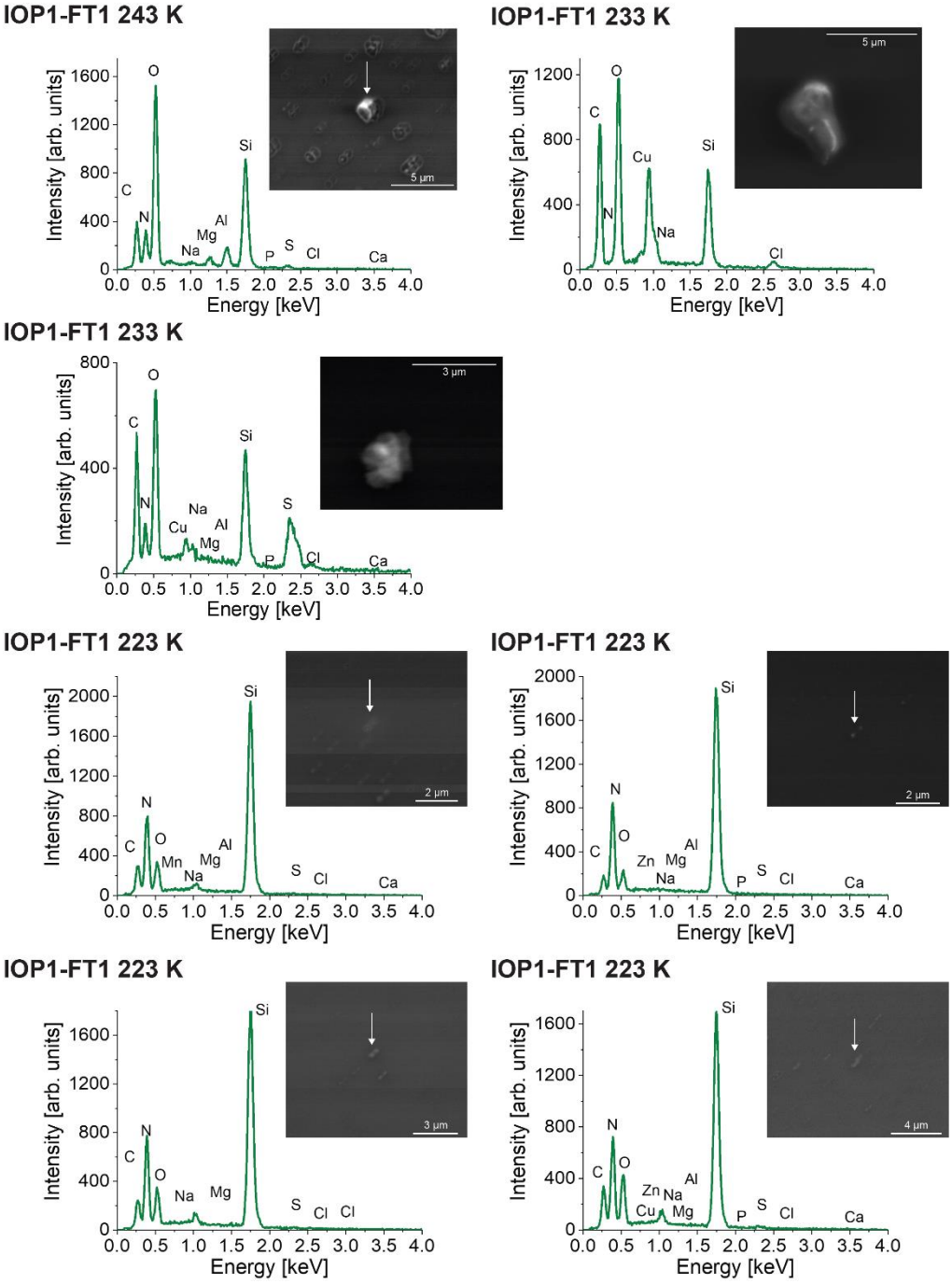


**Figure S9: EDX spectra of identified INPs from particles samples collected during IOP1 under free troposphere (FT) conditions with corresponding SEM obtained particle image. Si and N signals stem from the substrate ($Si_3N_4$ coated silicon wafer chips) and the chamber/holder (Al).**

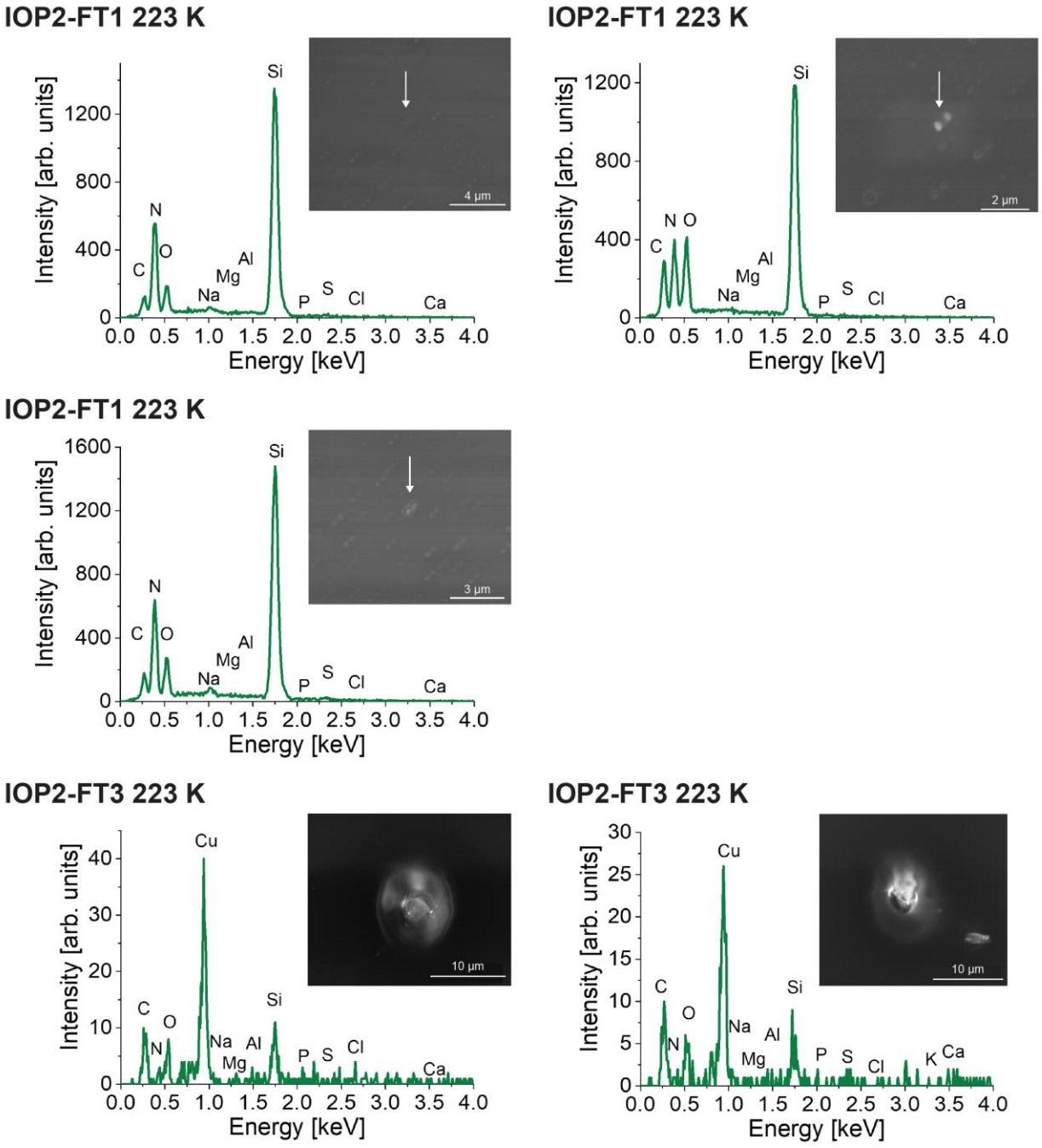


**Figure S10: EDX spectra of identified INPs from particles samples collected during IOP2 under free troposphere (FT) conditions with corresponding SEM obtained particle image. Si and N signals stem from the substrate ($Si_3N_4$ coated silicon wafer chips) and the chamber/holder (Al).**

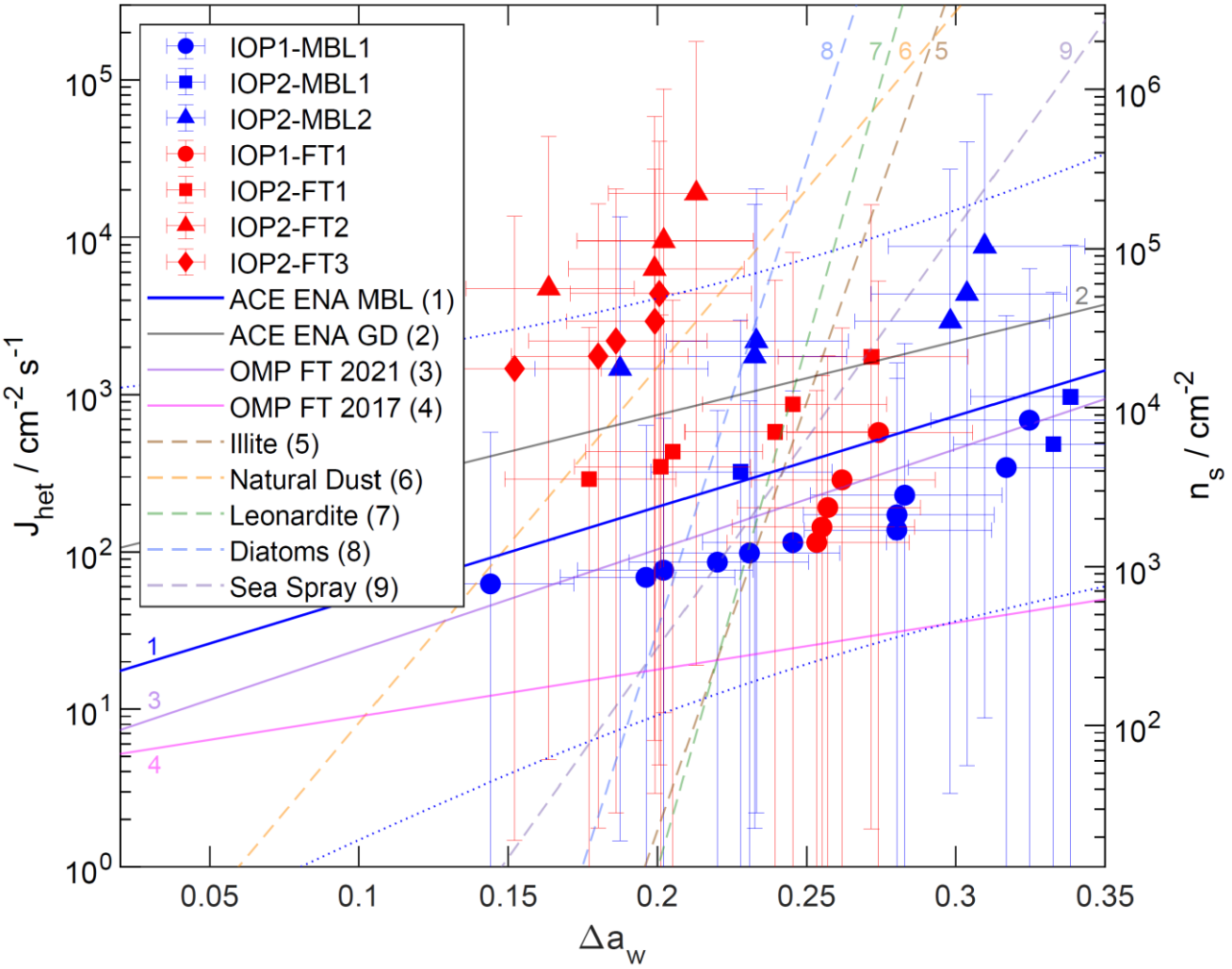


**Figure S11:** **Immersion freezing (IMF) data of examined ACE-ENA particle samples (solid symbols) and of previous studies (colored lines) as given in legend. Heterogeneous ice nucleation rate coefficients ($J_{het}$) and ice nucleation active sites (INAS) density ($n_s$) are presented as a function of the water activity criterion $\Delta a_w$. Error bars include uncertainties in temperature, humidity, and surface area. Blue solid line represents a linear regression to the newly derived MBL IMF data. Solid black, magenta, and purple lines represent $J_{het}$ and $n_s$ IMF derived from accompanying ACE-ENA ground site INP measurements (ACE-ENA GD), from the Observatory of Mountain Pico (OMP) measurements under free tropospheric (FT) conditions in the Azores on a neighboring island (PMO FT 2017, 2021; (China et al., 2017; Lata et al., 2021)). Please note that only $J_{het}$ was reported for OMP FT 2021 (Lata et al., 2021). Water activity-based IMF $J_{het}$ and $n_s$ for other INP types are given as dashed colored lines as indicated in legend.**

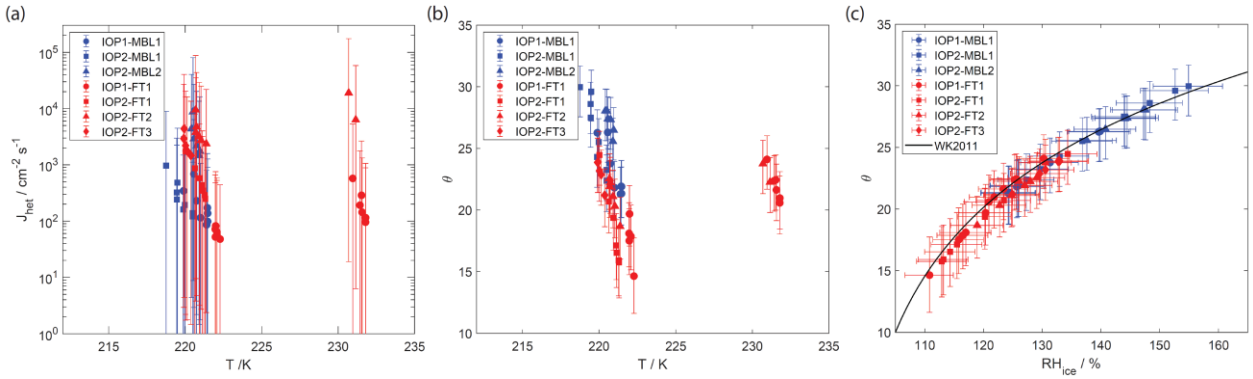


**Figure S12: Deposition ice nucleation (DIN) data of examined ACE-ENA MBL and FT particle samples in blue and red colors, respectively. (a) Heterogeneous ice nucleation rate coefficients ($J_{het}$) as a function of temperature. (b) Contact angles ($\theta$) corresponding to $J_{het}$ values shown in (a). (c) $\theta$ values for relative humidity with respect to ice ($RH_{ice}$) under which DIN was observed. Solid line represents the DIN parameterization by Wang and Knopf (2011).**

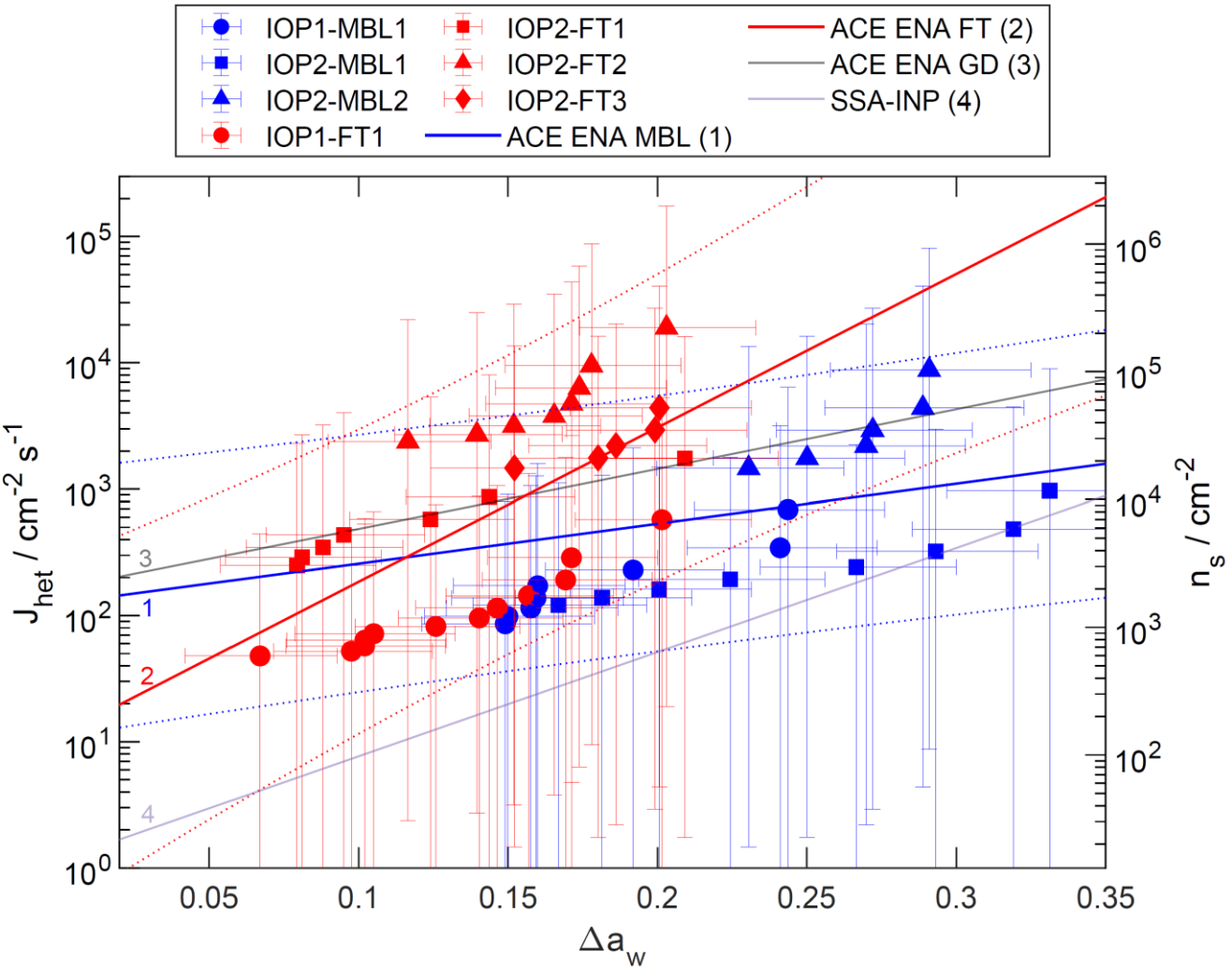


**Figure S13: Deposition ice nucleation (DIN) data of examined ACE-ENA MBL and FT particle samples (blue and red symbols, respectively). Heterogeneous ice nucleation rate coefficients ($J_{het}$) and ice nucleation active sites (INAS) density ($n_s$) are presented. Error bars included uncertainties in temperature, humidity, and surface area. Blue and red solid and dotted black lines represent linear regression fits and associated fit uncertainties for MBL and FT particle samples, respectively. Black line represents the DIN ABIFM parameterization derived from ground site ACE-ENA INP measurements. Purple line represents the water-activity based DIN sea spray aerosol parameterization from Alpert et al. (2022).**

## References

NASA Goddard Space Flight Center, Ocean Ecology Laboratory, Ocean Biology Processing Group. Moderate-resolution Imaging Spectroradiometer (MODIS) Aqua Global Level 3 Mapped SST. Ver. 2019.0. PO.DAAC, CA, USA. Dataset accessed [2023-03-21] at https://doi.org/10.5067/MODSA-MO4D9.

NASA Goddard Space Flight Center, Ocean Ecology Laboratory, Ocean Biology Processing Group. Moderate-resolution Imaging Spectroradiometer (MODIS) Aqua Chlorophyll Data; 2022 Reprocessing. NASA OB.DAAC, Greenbelt, MD, USA. doi: 10.5067/AQUA/MODIS/L3B/CHL/2022. Accessed on 03/21/2023